Atacama Large Millimeter Array

ALMA Single Dish Imaging Parameters, a Comparison of Observed Beams to Predicted Beams, and a Demonstration of the Method for Measuring Jy/K

SCID-90.04.00.00-0001-A-REP
Version: A
Status: Draft
2014-08-19

Prepared By:		
Name(s) and Signature(s)	**Organization**	**Date**
C.L. Brogan, T.R. Hunter	NRAO	2014-08-19
Approved By:		
Name and Signature	**Organization**	**Date**
A. Wootten L. Testi	NRAO INAF-Osservatorio Astrofisico di Arcetri	
Released By:		
Name and Signature	**Organization**	**Date**
Stuartt Corder	JAO	

ALMA Single Dish Imaging Parameters, a Comparison of Observed Beams to Predicted Beams, and a Demonstration of the Method for Measuring Jy/K

C.L. Brogan & T.R Hunter (August 19, 2014)

ABSTRACT

We present a comprehensive analysis of our experiments on imaging 39 ALMA single dish datasets of SD amplitude calibrators (3c279, Mars, and Uranus) from Bands 3, 6, and 7. We provide recommendations on the choice of parameters to use in the CASA task `sdimaging`, including `gridfunction`, `convsupport`, and `cell`. In order to resolve the problem that the post-imaging primary beam size is not currently available (making it impossible to derive the integrated flux density for resolved sources), we define a method to accurately predict the FWHM beam size of an image as a function of the image parameters chosen, the frequency, and the receiver band. For this prediction we use the band-dependent TICRA optical models, which we demonstrate are a good representation of the actual beam, compared with existing Astroholography, and certainly better than the standard Gaussian or truncated Airy disk approximations. The TICRA model images in Bands 4, 6, and 7 are consistent with the FWHM of the intrinsic antenna beam being 1.15λ/D. The predicted radial profile of the post-imaging beam matches the astroholography result to about $\pm 6\%$ in terms of the measured flux density out to the -10 dB point. Finally, we demonstrate the procedure for using images of amplitude calibrators to derive the correct antenna gain factor (Jy/K) to be used to convert images of science targets from brightness temperature units into intensity units (Jy/beam), and we plot the results from all our datasets. For faint sources with $T_{\rm B} << T_{\rm sys}$ (i.e. quasars and small planets), the derived gain factor shows the expected trend as a function of frequency with a residual standard deviation of less than 4%. However the absolute value of the Jy/K factor is ultimately dependent upon the values adopted for the intrinsic antenna beamsize and the non-linearity correction factor for the 3-bit baseband samplers and the 4-bit requantizers in the ACA correlator. If we accept the 1.15λ/D result from the TICRA models, then we derive a non-lineary correction factor of 1.30 ± 0.05 for continuum observations. Brighter sources (e.g. Mars at Band 6 and above) cannot be used to determine the gain factor due to the current implementation of the non-linearity corrections in the ACA correlator.

1. Executive Summary

We have processed 39 ALMA ACA single dish datasets (each with 1-4 usable antennas) from Bands 3, 6, and 7 with the CASA 4.2.0 task `sdimaging`, exploring a systematic grid of control parameters for both the SF and GJINC gridding functions. We tabulate the useful ranges for the image `cell` size as a function of the control parameters (`convsupport` and `gwidth/jwidth`). In order to resolve the long-standing problem that single-dish images do not contain a beam size in the header, we worked extensively to develop a script-able method to accurately predict the beam size of an image as a function of the image parameters chosen, the frequency, and the receiver band. We wrote python functions to simulate the convolution of the telescope primary beam with the gridding function and the spatial sampling interval and compared the predicted profiles and FWHM to the measured profile and FWHM of point sources in actual images. We find that using a Gaussian approximation to the beam expected for an edge taper of -10 dB (FWHM = $1.13\lambda/D$) as the input model leads to a systematic overestimate of the actual beamsize by several percent in all bands. In contrast, using the profile of the TICRA electromagnetic model beam images as the input model brings the predicted beamsizes into better agreement with the images, with residual differences of about 3 percent, depending on the specific antenna. In terms of beam area, these residuals are doubled to about 6 percent when considering the error in the integrated flux density measurement and hence our measurement of the Jy/K antenna gain factor.

In the course of our observations, we found that the current correction implemented in the ACA correlator to correct for the non-linearity of the IF digitizers and the ACA requantizers adversely affects the observations of bright calibrators (e.g. Mars at Band 6 and above). Because it applies a single correction per subscan, it cannot adapt to raster mapping data which the total power varies substantially when the target passes through the beam in the course of a single (row) subscan (CSV-2810). Thus the recorded intensity will be compressed from reality. This problem will also plague science targets (with either bright continuum or bright spectral lines) and must be dealt with before bright SD Early Science can begin in earnest.

As a result of our comprehensive study, we make the following conclustions and recommendations:

1. To encourage a good uniform quality of single dish images, the default values to use in the CASA task `sdimaging` should be set to:
   - `gridfunction` = 'SF'
   - `convsupport` = 6
   - `cell` = beamsize/9.0
2. An improvement is urgently needed in the non-linearity correction implemented in the ACA correlator (see CSV-2810) before SD Early Science can begin in earnest. At

present, the correction can only be applied once per subscan, whereas once per dump is necessary when scanning calibrators and science targets with strong continuum emission if we are to achieve the promised level of flux calibration accuracy. Furthermore, the correction must be applied on a spectral basis when scanning science targets with bright spectral lines. For fainter sources, we find that the non-linearity correction for continuum observations with the ACA correlator is 1.26 ± 0.05, based on our imaging analysis that compares the predicted Jy/K factor to the measured Jy/K factor,

3. The TICRA models provide a good prediction of the antenna beam width compared to observations in Bands 6 & 7. Likewise, a convolution of these models with the gridding function and sky sampling provide a good prediction of the image beam width, and should be written to the image header. Unlike in the other bands, the beam width of the Band 3 TICRA models show an anomalous frequency dependence. Furthermore, the models were generated for the old version of the Band 3 warm optics. We recommend that the project procure new optical models for Band 3 beam from TICRA so that we can complete a consistent analysis in the band. Dirk Petry recently obtained a quote of 20000 Euros for TICRA to complete this task, which is currently underway. The importance of this model is underscored by the observational results in CSV-3057 which confirm the anomalous decline in the frequency-normalized beam width above $\sim$105 GHz. In the interim, we recommend that the 125 GHz TICRA model of Band 4 be used at Band 3 with appropriate frequency scaling, as we have done in the plots in § 6.

4. The TICRA models should be used as the ALMA primary beam pattern in the interferometric tasks of CASA, rather than the current truncated Airy disk. Initially, this may need to be implemented using an axisymmetric radial profile rather than the full images, in order to avoid long computation times in the `clean` task. This option has been requested in CAS-3532, and the CASA developer expects to start work on it soon.

Contents

2. Motivation

Single dish (SD) observations for spectral line projects at Bands 3, 6, and 7 were first allowed in the Cycle 1 call for proposals. Over a dozen accepted Cycle 1 projects require these observations to be combined with ACA and 12 m array data in order to recover the large spatial scales. Moreover, though we don't yet know the demand for spectral line SD data for Cycle 2 it is likely the demand will be even higher. However, as of October 2013, this observing mode was still being commissioned and several major questions were still outstanding ranging from (1) how the data should be acquired, (2) how the SD images should be created, (3) how best to convert from Kelvin to Janskys, and (4) how best to feather the SD data with the interferometer data. Therefore, it was essential to answer these questions before the CASA guide on the M100 Science Verification data could be completed (the first to attempt a complete combination of SD+7m+12m array data), or indeed any SD data is delivered to PIs. In this memo we address question (2), and attempt to resolve a key problem for (3), namely that SD images created in CASA (as of the 4.2.1 release) do not have any beam information. This means that no flux densities can be measured from them. Indeed, this is not a fault of CASA as no detailed *observational* study of the ALMA primary beam properties has been forthcoming thus far. Additionally, the beam that needs to be inserted into the SD image is not simply the beam that results from the antenna/optical design,

but rather that beam convolved with the imaging convolution function, and any broadening present due to undersampling of the beam response by the observed raster pattern.

As part of the commissioning process, the following basic calibration scheme was devised:

1. Observe the spectral line science target and a compact pseudo-continuum calibration target using the same scan spacing (5x3 samples per beam) and the same spectral line setup. The calibration data rasters should be six half-power beamwidths (HPBW) wide. The purpose of the compact pseudo-continuum observation of a source of known flux density (hereafter called the SD-cal observation/data for short) is to determine the K/Jy conversion factor, and in principle to determine/verify the primary beam size/shape. It is executed in a separate scheduling block to allow for the fact that an appropriate calibrator is often not available at the same LST range as the science target.

2. In CASA 4.2, the "science" and "calibration" data are reduced using the generateReducScript method with step='SDcalibLine' or 'SDcalibCont', respectively. The former choice uses the observed off position for calibration and does baseline subtraction, while the latter uses the edges of the map for calibration and does no baseline subtraction.

In the course of assessing this basic scheme, it has become clear that the SD-cal data cannot in general be used to accurately derive the primary beam size/shape because it is very challenging to achieve adequate S/N using the current pseudo-continuum technique (lacking a nutator). Indeed, we find that even in excellent weather, the pseudo-continuum technique currently in use is too noisy for all but the strongest quasars at Band 3 and at higher frequencies a strong and *compact* planet must be used instead. Even then, the weather conditions must be better than the average adopted for each band to achieve high S/N. For this reason our focus has changed to only using the SD-cal data to measure the Jy/K conversion factor, and to develop a way to *predict* the primary beam size as a function of frequency rather than try to measure it for each individual science project.

In this memo we (1) Describe the factors that influence the final post-imaging beam including the gridding function (spheroidal and GJINC are considered), sampling on the sky, and the intrinsic telescope beam pattern (§3). For the latter we compare in detail TICRA simulations and astroholography results; (2) Describe a method for predicting the post-imaging beam (§4); (3) Show the results of image analysis, including the use of spheriodal and GJINC gridding functions on a wide range of SD amp-cal test data, including the results from both beam-fitting and beam-prediction (§5); (4) Give a prescription for calculating the Jy/K conversion factor along with analysis of its value for a wide range of test data (§6); and finally (5) We review what is currently used for the primary beam shape in CASA interferometric imaging and suggest an alternative (§7).

NOTE: In doing our analysis we assume that the basic SD Cycle 1 and 2 observing scheme is now fixed, namely that rasters are acquired such that ~ 5 samples per beam (according to the lowest frequency spw) are taken in the scan direction and ~ 3 samples per beam in the orthogonal direction. This scanning pattern has been decided upon primarily due to the current limitations on the ACA correlator's data rate. **if the observing scheme is changed the analysis presented here will also have to be revisited**. Additionally, all of our analysis has taken place on data taken in RA, Dec coordinates, since this is the coordinate scheme adopted by the observatory (see ICT-2499). Initial tests of Az-El vs. RA, Dec suggests that this choice has little effect on the SD image quality. The python functions that we have written are available in `analysisUtils.py` and are listed in the appendices along with a pointer to their online documentation. The scripts that call these functions to analyze specific datasets are also described and will be made available on the JIRA ticket CSV-2892.

3. Elements that influence the beam

In order to measure flux densities of sources in a radio image, the image must contain accurate *post-imaging* beam information in the header. The images produced by `sdimaging` do not (yet) contain a beamsize because it has heretofore not been known. The effective beamsize of a SD image depends on the following factors: (1) the gridding convolution function and its parameters, (2) the sampling interval on the sky, and (3) the intrinsic width and shape of the antenna primary beam.

3.1. Gridding functions

For various practical and intentional reasons, SD data are typically obtained on an irregular two-dimensional grid that must be resampled onto a regular grid prior to imaging. A summary of gridding functions used in radio astronomy is given by Mangum et al. (2007). Because the ALMA SD data are ultimately intended to be combined with interferometric data, and the overlap in spatial scales between the shortest 7m baselines and the (Gaussian-tapered) 12m antennas is rather limited, it is essential that the SD beam not be enlarged too much by the gridding process. In very general terms, the "spheroidal function" (SF) was recommended at the ALMA Single Dish and Array Combination workshop held in Grenoble in October 2012. A particular form of this function is used in interferometric imaging (Schwab 1981) and is implemented in AIPS and CASA, and is available to the CASA SD imaging task `sdimaging`. Additionally, the Gaussian times Jinc (GJINC) function has also been suggested as a suitable gridding function by the SD-combination working group. Thus we consider these to be the only viable current options for ALMA SD imaging. Below we describe how these two functions are implemented in CASA 4.2 and compare them with easy

to access `scipy` functions. Note in what follows the pixel size used to create an SD image is set by the "`cell`" parameter. When another parameter is defined in terms of a "pixel", this refers to the angular size set in the `cell` parameter.

3.1.1. Spheroidal function

Spheroidal functions are described in Rhodes (1970). The spheroidal function of order 0 (typically referred to as n=0) is non-zero only over a finite domain, typically defined as 0 to 1, but of course the profile shape can be scaled to any radius. In practical terms, this means that it reaches zero at a finite value of x, very much unlike the infinite wing of a Gaussian. The spheroidal function implemented in CASA can be found in the Fortran source code file `casacore/scimath_f/grdjinc1.f`, in function `grdsf`. It is an implementation of the approximation developed by Fred Schwab for AIPS for the specific case of a support width of 6 (i.e. m=6 in VLA Computer memo 156) and a weighting exponent α=1. This support width should not be confused with the `convsupport` parameter for the CASA SF grid function of `sdimaging`, which does not change the shape of the function, only its angular size. The default value of `convsupport` in `sdimaging` is 3; in our analysis we consider values of 3, 4, 5, and 6 (only integer numbers are allowed). A weighting exponent of α=1 is also implicitly assumed in the casa code (where it multiplies the convFunc by (1-nu*nu)**1 in STGrid.cpp in function STGrid::spheroidalFunc().

We have used scipy to generate an equivalent spheroidal function that can be used to predict the post-imaging beam from python. Specifically, we use `scipy.special.pro_cv(m,n,c)` to get the eigenvalue (cv), then call `scipy.special.pro_ang1_cv(m,n,c,cv,x)` to get the spheroidal function at a value of x. The coefficient values are: m=0, n=0, c=5.356$\pi/2$, where the value of c was found by matching the output of the Fortran code with the output of scipy. A plot of the agreement between the CASA implementation of SF and the scipy version (at the 0.1% level) is shown in Figure 1. Thus, we can be confident that our predictions for the gridded beamsize (Section 4) are using very nearly the same SF function as CASA.

3.1.2. GJinc function

The "GJinc" function is a Gaussian function multiplied by the Jinc function[1], then truncated to zero beyond some radius. In CASA, there are three control parameters for GJinc: `truncate`, `gwidth`, and `jwidth`. The `truncate` parameter specifies the truncation radius, which can be given in angular or pixel units, but the default of -1 means to truncate at the first null. The `gwidth` parameter is the HWHM for the Gaussian and

[1]Jinc(x) = J_1(x)/x where J_1(x) is a Bessel function of the first kind

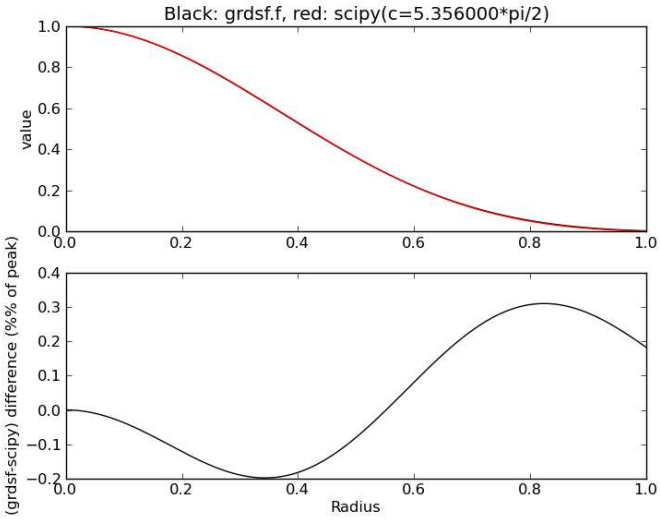

Fig. 1.— Comparison of SF function in CASA vs. scipy **Upper panel:** the black curve is the result of running the Fortran function grdsf extracted from CASA and compiled on a Linux machine. The red curve is the curve produced by scipy.special.pro_ang1_cv for coefficients specified in the text. **Lower panel:** shows the percentage difference between the two curves in units of the peak. This plot was created with the command:

`au.griddedBeam().plotgrdsf(plotfile='fred_vs_scipy.eps').`

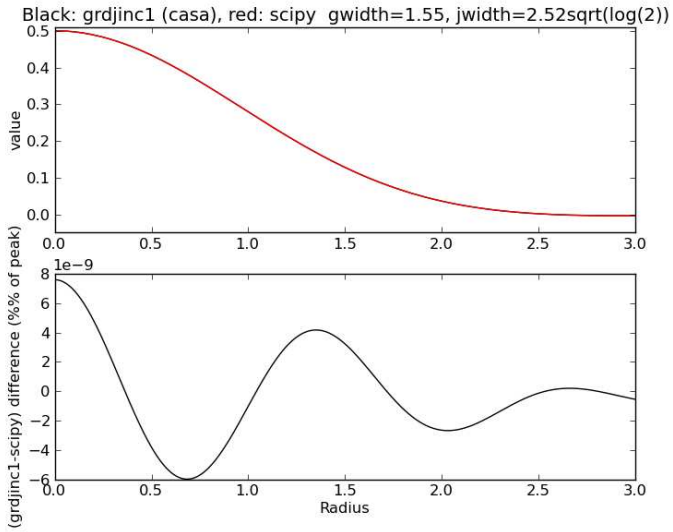

Fig. 2.— Comparison of GJINC function in CASA vs. scipy. **Upper panel:** the black curve is the result of running the grdjinc1 C++ function extracted from CASA and translated to python. The red curve is the curve produced by `scipy.special.j1(x)/x`. **Lower panel:** shows the percentage difference $\times 10^{-9}$ between the two curves in units of the peak. This plot was created with the command:

`au.griddedBeam().plotcasajinc(plotfile='jinc1_comparison.png').`

the default value is 2.52*sqrt(log(2))*pixel. The `jwidth` parameter is the control parameter for the Jinc function, and the default is 1.55 pixel. The GJinc function in CASA is implemented in C^{++} in the source file `asap/src/STGrid.cpp` in function `grdjinc1`. The function itself is a numerical approximation, which we have copied into analysisUtils function `au.griddedBeam().grdjinc1()` for comparison purposes with `scipy.special.j1`. The agreement between the two implementations is excellent, better than 1 part in 10^{10} as shown in Figure 2. Thus, we can be confident that our predictions for the gridded beamsize (Section 4) are using the same GJinc function as CASA. We have limited our analysis of the GJINC gridding function to the case where the *relative* relationship between the Gaussian and Jinc width parameters is maintained, to this end we define a "gwm" (gjinc width modifier) parameter such that in our analysis gwidth=2.52*sqrt(log(2))*pixel*gwm

and jwidth=1.55*pixel*gwm. Values of gwm=1.0 (i.e. the default), 1.5, 2.0, and 2.5 are explored in this memo.

3.2. Sampling interval on the sky

The ALMA control system is capable of obtaining back-and-forth raster scanning of a field in either equatorial or alt/az coordinates. The current data rate limitations of the ACA correlator (0.9 MB/s) restricts the dump time to ∼144 ms for FDM basebands (see CSV-2972). This sets a practical limit to the spatial sampling of about 5 points per primary beam in the scan direction if you want to map no slower than ∼1.4 beams per second. Due to other excessive overheads in the ACA correlator (CSV-2704), acquiring even small maps (6 beams by 6 beams) requires a long time to complete, and so the choice of sampling in the perpendicular direction, i.e. the space between rows, is typically set to 3 points per beam. These values were used in the commissioning datasets that we examine here. Because it is not possible to retrieve the sampling interval from the metadata of an dataset, we wrote a function `au.getTPSampling` to discern the sampling interval from the POINTING table of the measurement set.

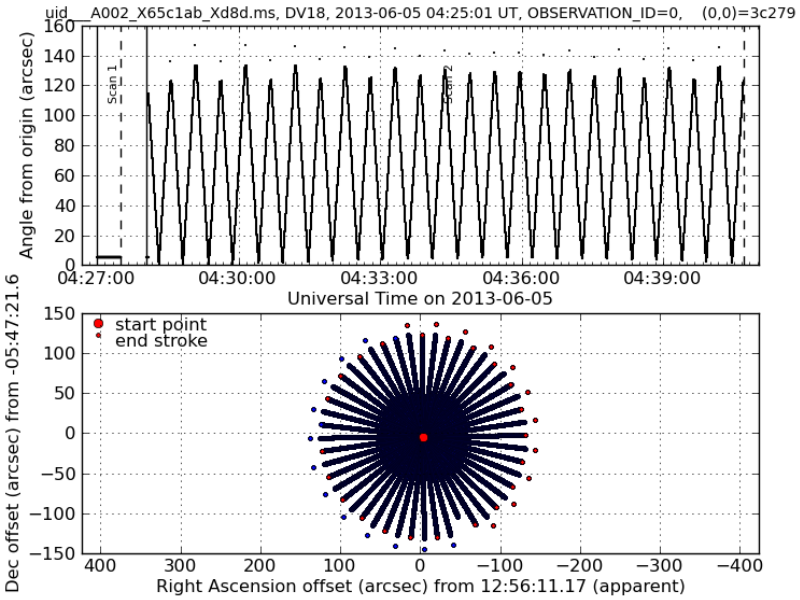

Fig. 3.— An example of the sky coverage and duration of a celestial holography map. This plot was created by running the following command:

```
au.getTPSampling('uid___A002_X65c1ab_Xd8d.ms',plotfile='dv18_sampling.png').
```

3.3. The ALMA 12m Primary Beams: TICRA models and Astroholography

In order to create high fidelity image mosaics with interferometers, the shape of the primary beam must be known to high accuracy. For a 40-element array, a knowledge to within

6% rms was recommended by Cornwell et al. (1993). This specification was drafted into the ALMA System Technical Requirements document (Morita et al. 2012) as Requirement #650 - Mosaic Image Dynamic Range:

"..primary beam shape must be known to better than ±0.06 of the primary beam response down to the -10 dB point (Sci Req #270)."

It is also listed in § 2.1.2 (Surface Setting and Primary Beam) of the Calibration Specifications and Requirements document (Butler et al. 2006). To be clear, the 6% specification corresponds to power. In other words, the voltage pattern must be known to better than 3% down to the -10 dB point. With the exception of Figure 23, the present document displays images and profiles of the power patterns. We will henceforth refer to the portion of the antenna beam above the -10 dB response point as the "main beam area".

As a step toward this goal, electromagnetic models of the ALMA front ends coupled to the ALMA DA and DV antennas performed by the Danish company TICRA[2] (Pontoppidan 2007, Sørensen & Pontoppidan 2010), and the resulting images of the farfield complex beam (voltage) patterns (Petry 2012) are available in the CASA data repository (in the directory `/usr/lib64/casapy/data/alma/responses`). These can be converted into power patterns using `au.complexToSquare`, which calls the CASA `immath` task. **Note that the current Band 3 model beams were computed for the old version of the warm optics, when one of the mirrors was a flat mirror, rather the version that is on all antennas at the high site as a result of the change request ALMA-40.01.03.00-013-A-CRE.**

[2]www.ticra.com

Table 1. Astroholography datasets used in Figures 4, 5 and 6

Band	Execution block[a]	Spw center frequency[b]	Start Date/Time	Antenna
3	uid___A002_X67509f_X744	98.20 GHz (LSB)	2013-06-12 04:14	DA48
3	uid___A002_X69ec79_X9f8	98.20 GHz (LSB)	2013-07-05 01:16	DV17
3	uid___A002_X680f8a_X310	98.20 GHz (LSB)	2013-06-18 23:29	PM04
6	uid___A002_X6643c8_X49	230.58 GHz (LSB)	2013-06-17 01:35	DA48
6	uid___A002_X680f8a_X399	230.58 GHz (LSB)	2013-06-19 00:14	DV17
6	uid___A002_X6643c8_X49	230.58 GHz (LSB)	2013-06-17 01:35	PM04
7	uid___A002_X65c1ab_X950	333.84 GHz (LSB)	2013-06-05 02:54	DA48
7	uid___A002_X65c1ab_X950	333.84 GHz (LSB)	2013-06-05 02:54	DV17
7	uid___A002_X65b087_X810	333.84 GHz (LSB)	2013-06-04 04:31	PM04

[a]The measurement sets can be found at scops01.sco.alma.cl:/mnt/scops/data/data/tsawada/astroholo/

[b]Of the two TDM full-polarization windows in the sideband

The new warm optics are described in a separate TICRA report (Albertsen 2009).

As part of commissioning, measurements of the antenna beam pattern at Bands 3, 6, and 7 have been obtained with celestial holography (a.k.a. astro-holography) scans of bright quasars (CSV-98, CSV-466, CSV-1348). Celestial holography is performed with the PrimaryBeam.py script (in AIV/science/scripts/R9.1.1_WORKING), which takes diameter scans through the quasar at a sequence of 24 position angles, i.e. every 180°/24=7.5°. A typical invocation of the command is:

```
PrimaryBeam.py -b 3 -o 3c279 -N 24 -P 4 --referenceAntennas 1
```

The resulting coverage pattern is shown in Figure 3. A paper describing the use of the phase pattern from these data to measure the gravitational deformation vs. elevation of all ALMA antennas is currently in draft form (Sugimoto et al. 2014). In this paper, the gridding convolution function used to convert the star-like pattern of observed points into a rectangular grid in azimuth and elevation is described as a Gaussian profile with a width equal to half the expected primary beam. Initially, we throught that we should convolve the TICRA beam patterns with this Gaussian prior to computing the square of their amplitude in order to compare them with the astroholography beam patterns. However, consultation with Robert Lucas (the author of the CLIC software) revealed that a gridding correction is applied as a taper in the antenna aperture domain prior to transforming the data back to the beam domain, hence the effect of this convolution should be removed in the beam images output by CLIC.

The ALMA receivers were designed to illuminate the subreflector with a -12 dB edge taper in the Gaussian beam approximation, which equates to about -10 dB in the physical optics analysis as described in the Front End Optics Design Report (Carter et al. 2007). Accounting for the 0.5% beam-narrowing effect of the 0.75 m central obstruction (Schroeder 1987), a -12 dB taper should result in a FWHM beamwidth of 1.151λ/D, whereas a -10 dB taper should result in 1.131λ/D (Baars 2007). Thus, the true ALMA beam FWHM likely lies somewhere near or between these two values. In Figure 4, we show an overlay of the horizontal and diagonal cuts through a celestial holography beam image (polarization-averaged) at a central frequency of 98.2 GHz, the TICRA model at 100 GHz scaled in angle by the frequency ratio, a Gaussian profile of FWHM $1.131\lambda/D$, and the Airy disk for a 10.7 m aperture (which is currently used as the ALMA 12 m beam model in CASA). For simplicity, we show only the X polarization results, and note that the TICRA models do not differ much between the X and Y polarizations. The TICRA model provides a good match to the data, even as far as the -20 dB point in some cases. The simple Gaussian profile slightly undershoots the TICRA beam from the peak to the -7 dB point. Beyond that point, it then overshoots the TICRA beam, particularly in the area near the first null.

To be more quantitative, the residual profile (with respect to the astroholography) is shown in lower left panels. In Band 3, the TICRA model matches the observed DV

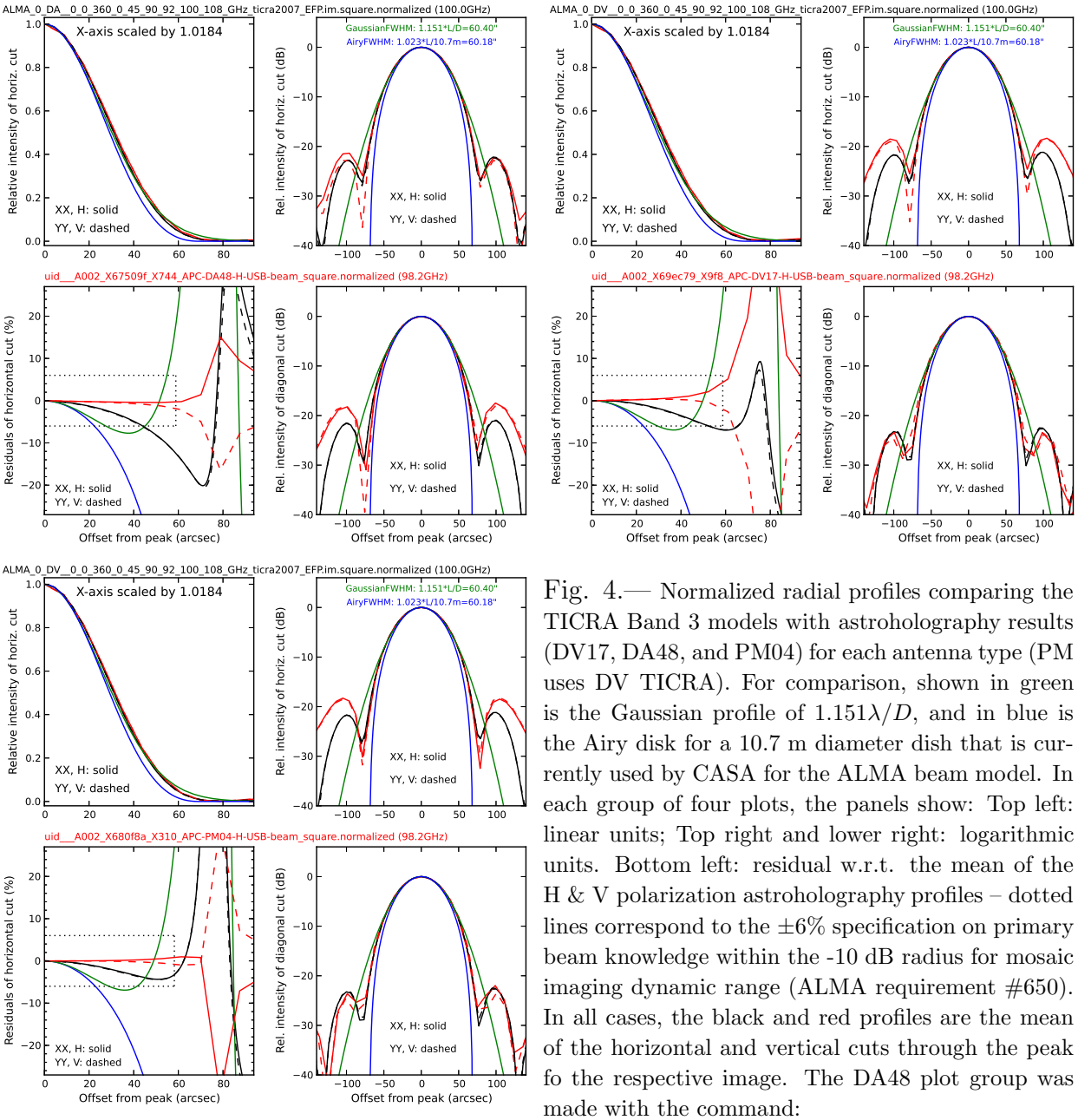

Fig. 4.— Normalized radial profiles comparing the TICRA Band 3 models with astroholography results (DV17, DA48, and PM04) for each antenna type (PM uses DV TICRA). For comparison, shown in green is the Gaussian profile of $1.151\lambda/D$, and in blue is the Airy disk for a 10.7 m diameter dish that is currently used by CASA for the ALMA beam model. In each group of four plots, the panels show: Top left: linear units; Top right and lower right: logarithmic units. Bottom left: residual w.r.t. the mean of the H & V polarization astroholography profiles – dotted lines correspond to the ±6% specification on primary beam knowledge within the -10 dB radius for mosaic imaging dynamic range (ALMA requirement #650). In all cases, the black and red profiles are the mean of the horizontal and vertical cuts through the peak fo the respective image. The DA48 plot group was made with the command:

```
au.overlayCuts(
  'ALMA_0_DA__0_0_360_0_45_90_92_100_108_GHz_ticra2007_EFP.im.square.normalized',
  'uid___A002_X67509f_X744_APC-DA48-H-USB-beam_square.normalized',
  'uid___A002_X67509f_X744_APC-DA48-V-USB-beam_square.normalized',
  frequency2=98.2, frequency3=98.2, stokes1='both', panels=4,
  row1='auto',row2='auto',row3='auto',column1='auto',column2='auto',column3='auto',
  plotrange=[0,140*0.67,-0.02,1.03],plotrange2=[-140,140,-40,6],
  plotfile='band3_DA_profiles_USB.png', scaleToArcsec=True, diameter=10.7,
  gaussian=au.primaryBeamArcsec(frequency=98.2,showEquation=False) )
```

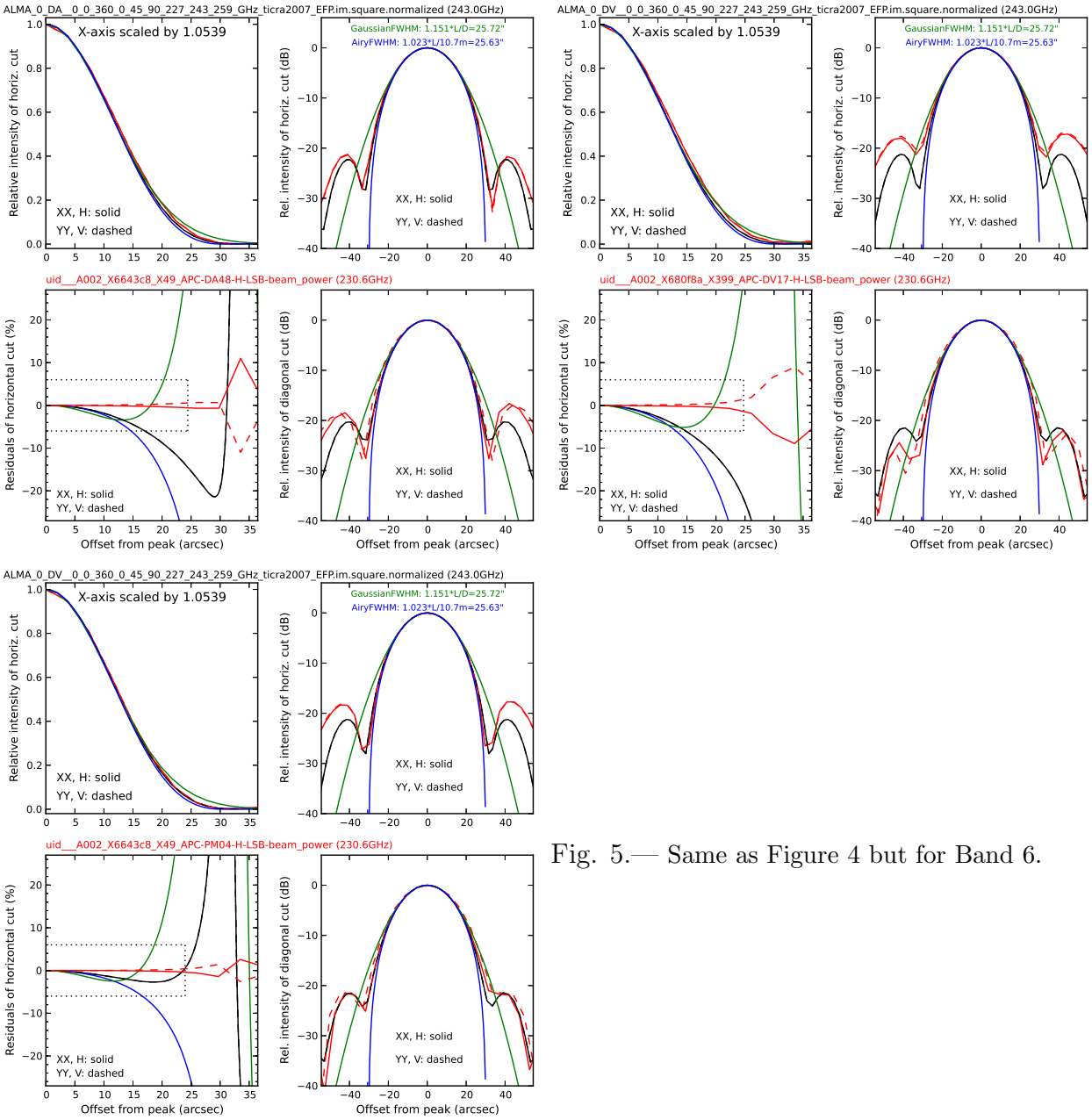

Fig. 5.— Same as Figure 4 but for Band 6.

and PM antenna patterns to within the 6% specification out to the -10 dB point. The TICRA DA model provides a somewhat poorer match to the DA antenna astroholography, but remains within about 12% of the observations across the specified main beam area. A similar set of example plots for Bands 6 and 7 are shown in Figure 5-6. The agreement between the model and observation is somewhat worse in Band 6 but remains in specification for the PM antenna. The specification is not met in Band 7, however the quality of the individual astroholography scans become worse at higher frequency due to fainter quasars and higher system temperatures. We caution that there are significant differences seen in the low-level details between antennas of the same type, and between different datasets

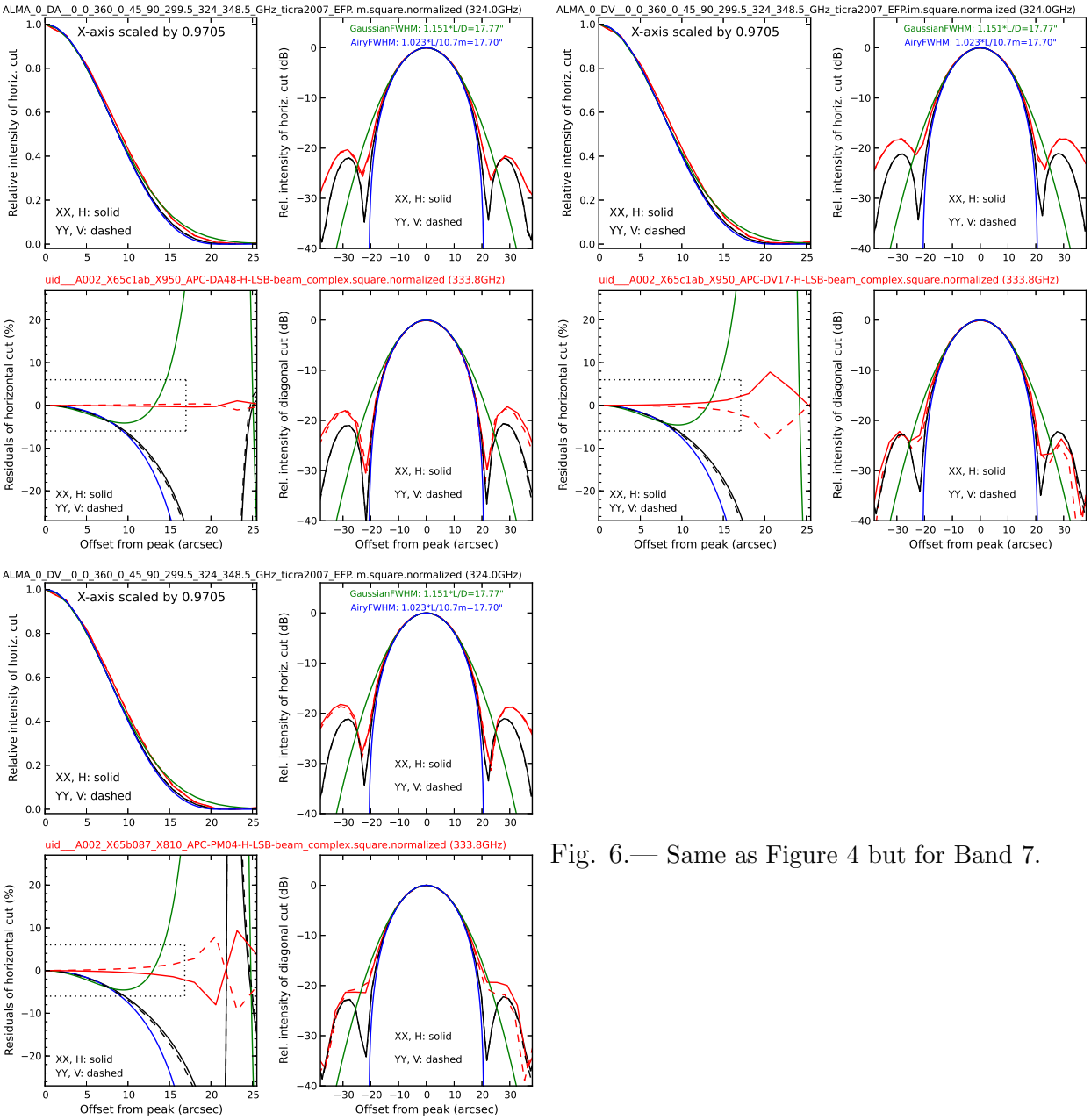

Fig. 6.— Same as Figure 4 but for Band 7.

of the same antenna. To see the variety, a full grid of profiles (generated by the script holo_ticra_profiles.py) can be found linked from a table on the summary wikipage: https://safe.nrao.edu/wiki/bin/view/ALMA/NAASC/Memo114Appendices. The datasets used for all of these plots in Figures 4-6 are tabulated in Table 1. The holography image data are located in the JAO scops cluster directory: /mnt/scops/data/data/dgunawan/PrimaryBeams.

Another way to compare the the TICRA models and the astroholography data is to view the low-level details in the two-dimensional beam images. Using the same images that

went into constructing Figures 4-6, an example for each antenna type is shown in Figure 7, 8, and 9 for antenna types DV, DA, and PM, respectively. Note that the intensities beyond the first null are strongly azimuthally-dependent, due primarily to the difference in the feed leg structures. The DA feedlegs extend to the edge of the dish, meaning that they do not scatter radiation twice (unlike the other antennas). As was already seen in the profile plots, there are also differences in the low-level details apparent between antennas of the same type, and between different datasets of the same antenna. To see the variety, a full grid of images (generated by the script holo_ticra.py) can be found linked from the table on the summary wikipage:
`https://safe.nrao.edu/wiki/bin/view/ALMA/NAASC/Memo114Appendices.`

A final quantitative comparison of the TICRA models with the astroholography results can be made by comparing the FWHM of the beam images. In Figure 10, we show the FWHM of the models and observations vs. frequency, computed with three different methods. To facilitate comparison across bands, the FWHM has been normalized by the expected width of the Gaussian profile of $1.131\lambda/D$ (i.e. the one that was shown in Figures 4-6). Regardless of method, the astroholography images all show systematically wider FWHMs than the TICRA models, by 2-5%. The TICRA models in Band 3 show a curious discrepancy compared to the models in Bands 4-7. The FWHM of the Band 3 model beams do not follow the trend from high frequency, with the 116 GHz TICRA model being more discrepant, and the 84 and 100 GHz models being less discrepant. Which one is more correct (if any) is unclear because we lack astroholography data near 116 GHz. We also see that the naive approach of fitting a Gaussian (shown in the top panel of Figure 10) produces the narrowest result. This happens because a plain Gaussian fit will undershoot the inner part of the beam while it simultaneously overshoots the outer part of the beam, as it goes through a null which the Gaussian cannot reproduce. In any case, the top panel of this plot is the one to use to compare to any ALMA beam measurements that were performed using naive Gaussian fitting, such as those reported in CSV-2897 and CSV-3057. Toward that end, we have included the Band 3 and 6 measurements from the 13-Dec-2013 report in CSV-2897 as green triangular points. More recent measurements from CSV-3057 are also included as red and black triangles. Interestingly, the drop in beam size near 116 GHz is confirmed by the 114 GHz result. Thus, further methodical exploration of the behavior of the beam width between 100 and 116 GHz is needed (see CAS-3057).

The middle panel of Figure 10 shows a modified fitting approach where only the pixel values greater than 45% of the peak are allowed in the fit. This produces a broader FWHM closer to reality as it ignores the data closer to the null.

The bottom panel of Figure 10 is our best determination of the FWHM using the function `au.getfwhm2`. We wrote this function (originally initiated by Brian Mason) to determine the FWHM of a beam image by examining all pixel values with no assumption about the detailed shape of the beam, only that it has a single main peak and is roughly

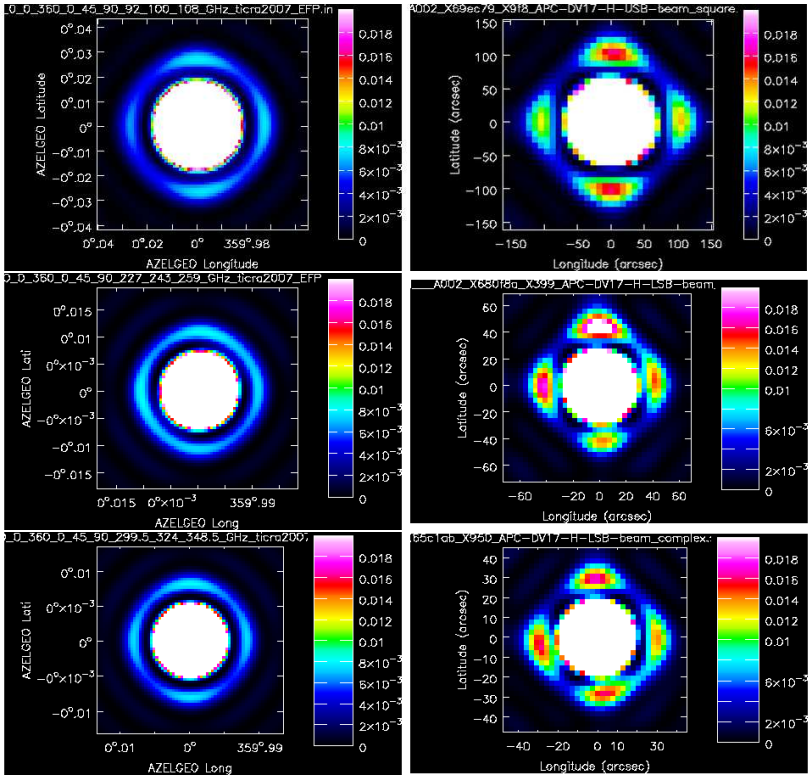

DV Band 3

DV Band 6

DV Band 7

Fig. 7.— Comparison of DV TICRA models (left) and astroholography (right) for DV17.

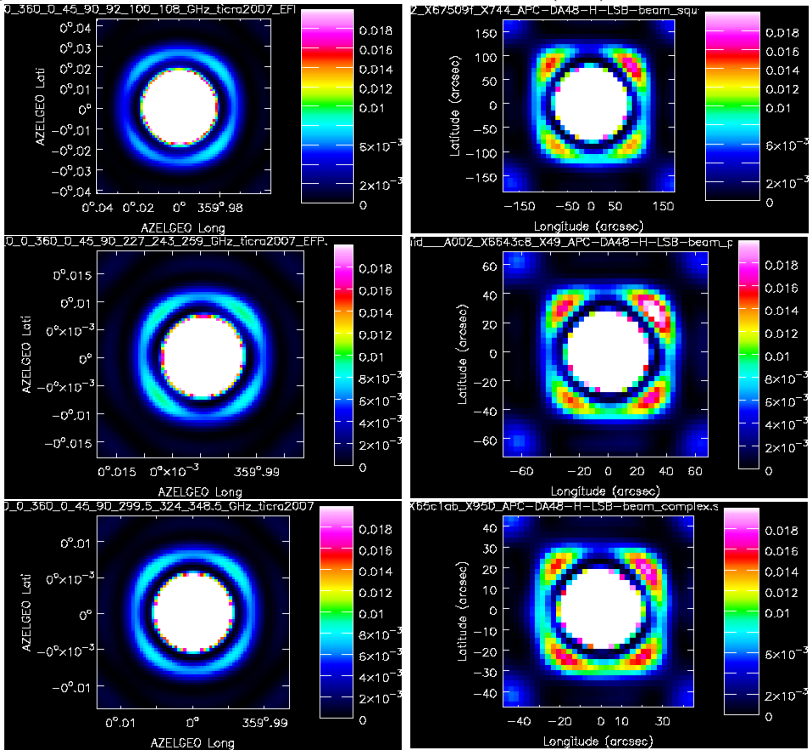

DA Band 3

DA Band 6

DA Band 7

Fig. 8.— Comparison of DA TICRA models (left) and astroholography (right) for DA48.

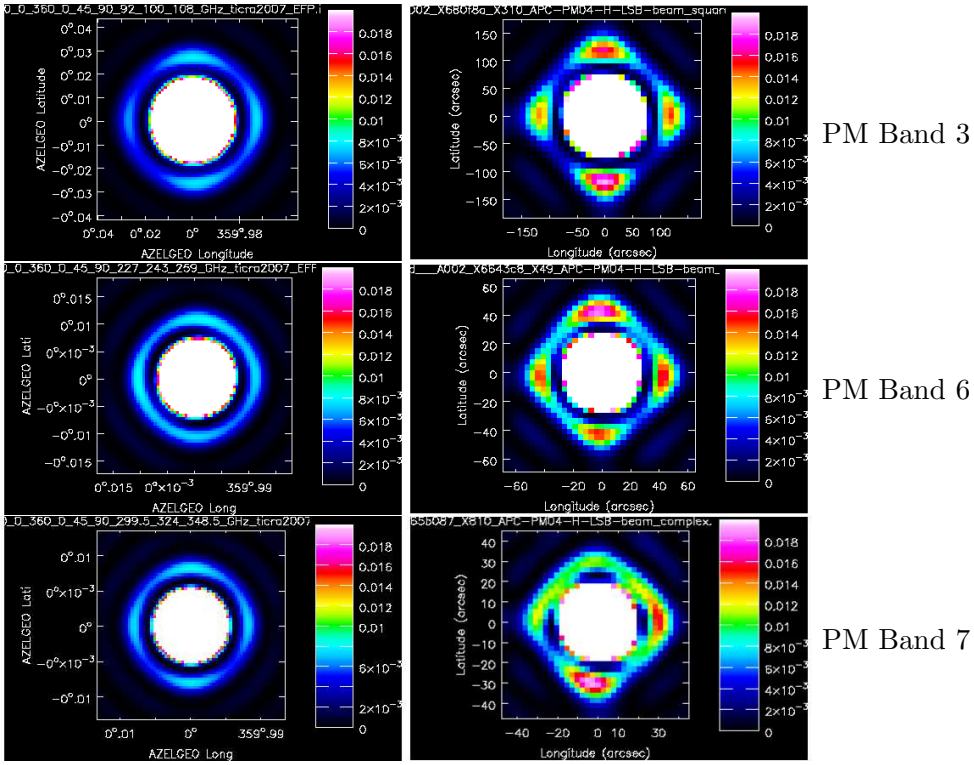

Fig. 9.— Comparison of DV TICRA models (left) and astroholography (right) for PM04.

azimuthally symmetric. It first finds the peak pixel, then forms a list of all pixels sorted by the radius from the peak. It then crunches this list (using `au.averageTheRepeatedValues`) by replacing all repeats of a radius with a single entry containing the mean value. It then uses `au.findFWHM` to subtract half the maximum from this profile, finds the (single) radius of the zero crossing. Finally, it doubles this radius to get the FWHM. If there are multiple zero crossings, as may occur with well-sampled but noisy data, then it will fit a line to the $\pm 20\%$ level and use the radius of the zero crossing of this line. For beams that are somewhat elliptical in shape, as they typically are, the FWHM that this function reports is effectively the mean diameter.

One caveat on the use of `au.getfwhm2` is that it will work less and less effectively for lesser sampled images than these. It does have an option to use the image centroid rather than the peak, which has the advantage of allowing the reference point to have non-integer pixel values. In this mode, there will be few (if any) repeats in the pixel radii from the peak, and results should be better for poorer sampled images. In practice, the centroid method yields very similar results to the peak method on images as well-sampled as these, and we have used the peak method for purposes of this memo.

4. Predicting the beam

In the previous section (§ 3.3), we demonstrated that the ALMA beamshape depends on the antenna type, and that the TICRA models provide a reasonably good model to the main beam shape. In the following two sections, we describe how we can use 1D profiles from these models to accurately predict the beamsize as a function of the `sdimaging` parameters.

4.1. Convolutions

The analysisUtils functions `au.sfBeam` and `au.gjincBeam` were written by us to predict the beam profile of a SD image at a specified frequency and choice of gridding parameters. They each begin with a representation of the ALMA telescope beam. One can select either a theoretical Gaussian profile, or the profile from a CASA image, such as a TICRA model image or a celestial holography image. For the Gaussian option, the width of the profile is set by the specified illumination taper (default: $T_e = 10$ dB). The relation between the width θ and the taper is implemented in `au.primaryBeamArcsec` as the equation 4.13 in the book by Baars (2007), $\theta = b\lambda/D$, where

$$b = 1.269 - 0.566\tau + 0.534\tau^2 - 0.208\tau^3$$
$$\tau = 10^{-0.05|T_e(dB)|}$$

Figure 11 shows an example of the calculations performed by `au.sfBeam` using the central row and column cuts through the peak of the TICRA model as the input beam. This task takes the model beam profile and convolves it with the gridding function, then convolves it with the boxcar function corresponding to the spatial sampling interval on the sky. On the resulting profile (and the intermediate profiles) it measures the FWHM by using `au.findFWHM` which works by subtracting half the maximum, forming a spline fit with `scipy.interpolate.UnivariateSpline` then calling `spline.roots` to find the two zero crossings and finally taking their difference. For the final profile, it also fits a 1D Gaussian and reports the FWHM. This final step is meant to simulate the result obtained by a user running the CASA task `imfit` on an image. These two estimates of the FWHM usually differ at a small level. By default, the central row and column are used to compute two independent estimates of the FWHM, and these results are averaged. In this case, the stokes parameter was set to 'both', and so the FWHM estimates for the XX and YY polarization TICRA images were separately computed and then averaged. Note that if the taper parameter is set to zero, `au.sfBeam` and `au.gjincBeam` will use an Airy disk as the input model. In this case, the Boolean `truncate` parameter indicates whether or not it should be truncated at the first null, which can be used to simulate the ALMA beam currently used by CASA (see §7), which is truncated at the 10% level.

4.2. The importance of gridding parameters and pixel (`cell`)

Currently in CASA, the `convsupport`, and `gwidth/jwidth` parameters for the SF and GJINC grid functions, respectively, can be defined either in units of the `cell` parameter (i.e. pixel size in the map) or in angular units (like arcsec). In either approach, it is important to be careful not to select a combination of `convsupport` or `gwidth/jwidth` with a `cell` that yields nonsense. For example, if cell size is too small for the chosen value of `convsupport` or `gwidth/jwidth`, you will get pixels containing no data because no sky measurements were taken close enough to their position. In Figure 13 (bottom panels), we show plots of how the post-imaging beam size changes as a function of the `convsupport` parameter for SF, and the `gwidth/jwidth` multiplier factor (gwm) for GJINC. These images demonstrate that larger gridding support sizes require more pixels per beam in the image in order to keep the post-imaging beam small. The top panels of Fig. 13 show the results from one-dimensional simulations of the effect of the convolution function on data acquired on a grid with a size of 3 samples per beam (i.e. the typical ALMA value used for the direction orthogonal to the scan direction). For each pixel the "weight" is determined by the amount of data on the sky that contributes to it, given the choice of gridding support parameters. For example, for the case of a poor combination of pixel size and gridding support parameter there can be large variation in the amount of data contributing to each image pixel. This effect is quantified by the weight variation (%) shown in Fig. 13. This simulated weight variation is directly analogous to the imagename.weight image created by `sdimaging`.

Together the top and bottom panels in Fig. 13 demonstrate the optimal range of pixels per beam to chose for a given gridding support size (`convsupport` for SF, or `gwm` for GJINC). Since the SD data are being taken for the purpose of combining with interferometric data, it is best not to grow the post-imaging beam too large as it reduces the effective area of overlap between the 12m SD antennas and the shortest baselines of the 7m array. However, a bit of smoothing increases the sensitivity of the image. We consider $10-20\%$ growth from the intrinsic antenna beam to be optimal. The top panels indicate the range of pixels per beam without significant variation in the amount of gridded data per image pixel, here we

Table 2. Useful range of pixels per beam as a function of sdimaging parameters

SF convsupport	GJINC gwidth/jwidth multiplier	pixels per beam
3	1.0	$4-6$
4	1.5	$6-8$
5	2.0	$7-10$
6	2.5	$8-12$

consider $< 2.5\%$ to be optimal. A summary of the useful range of pixels per beam as a function of the imaging parameters is given in Table 2. In the case of GJINC, the width of the convolution function is typically given by a non-integral number of pixels (see § 3.1.2), so the number of contributing pixels within the truncation radius varies in a quantized manner as the number of pixels per beam is increased. This leads to an irregular, non-monotonic increase in the weight variation in the 1D model, which also manifests as cross-hatching in the weight images in the 2D observations (see § 5 and Figures 16-17).

5. Imaging results

5.1. Datasets

The total power ACA datasets that we used in the final analysis are listed in Table 3. We actually examined dozens more that had various problems and had to be discarded, as well as many baseline correlator datasets acquired for comparison. In Band 3, both Mars and 3C279 were observed because both are sufficiently bright to obtain good pseudo-continuum images without a nutator, and allowed us to determine whether the sdimaging task does anything strange for ephemeris objects. In Band 6, no quasar is (currently) bright enough, so Mars was used, despite the fact that its size was growing to be a large fraction of the beam by the later datasets. Uranus would have been an ideal target but it was not a nighttime object by the time Mars had grown large. Neptune should also be (just) bright enough at the upper end of Band 6 but it has not yet been observed because it was exclusively a daytime target during the commissioning period (until mid-April 2014). Finally, in Band 7, Uranus was used since it was still available in the early evening during the first part of the commissioning period.

Unfortunately, a number of different antennas were employed in the tests, primarily due to various problems with individual antennas during the ongoing period of commissioning. All the datasets were acquired with the ACA correlator and in the RA/Dec coordinate basis of antenna scanning. All of the spectral windows analyzed had a bandwidth of 1-2 GHz and either 4080 or 124 channels. All the data were acquired after Nov. 10, 2013 when the fix for the ACA internal calibration problem was applied (PREQ-125, PRTSIR-656). The datasets were calibrated with the SD script generator: `es.generateReducScript(step='SDcalibCont')` with the most recent changes described in CSV-3009.

Table 3. ACA correlator datasets used in imaging tests

Execution block	Spectral window (center freq. GHz)	Start Date/Time	Antennas
3c279 Band 3 data			
[a] uid___A002_X725175_Xc3d	17, 23 (100.9, 114.7)	2013-11-11 10:45	DA62, DA64, PM01, PM04
[a] uid___A002_X725175_Xefd	17, 23 (100.9, 114.7)	2013-11-11 11:25	DA62, DA64, PM01
[a] uid___A002_X725175_X12c6	17, 23 (100.9, 114.7)	2013-11-11 12:05	DA62, DA64, PM01, PM04
uid___A002_X7d194b_Xb1a	17, 23 (115.1, 100.8)	2014-03-20 06:45	PM03, PM04
uid___A002_X7d44e7_X1035	17, 23 (86.0, 100.0)	2014-03-23 04:53	PM03, PM04
uid___A002_X7d44e7_X190a	17, 23 (97.5, 111.5)	2014-03-23 09:12	PM03, PM04
uid___A002_X7d44e7_X343b	17, 23 (115.1, 100.8)	2014-03-24 03:29	PM03, PM04
uid___A002_X7d6d46_X8c	17, 23 (115.1, 100.8)	2014-03-24 05:51	PM03, PM04
uid___A002_X7d6d46_X6c2	17, 23 (86.0, 100.0)	2014-03-24 07:18	PM03, PM04
uid___A002_X7d76cc_Xe58	17, 23 (97.5, 111.5)	2014-03-25 04:23	PM03, PM04
Mars Band 3 data			
uid___A002_X7a4b4d_X373	19, 23 (92.9, 105.0)	2014-02-04 05:29	DV10, PM01
uid___A002_X7a4b4d_X616	19, 23 (92.9, 105.0)	2014-02-04 06:21	DV10, PM01
uid___A002_X7a4b4d_X8bc	19, 23 (92.9, 105.0)	2014-02-04 07:11	DV10, PM01
uid___A002_X7a4b4d_Xb80	19, 23 (92.9, 105.0)	2014-02-04 08:23	DV10
uid___A002_X7d44e7_Xd67	17, 23 (86.0, 100.0)	2014-03-23 04:50	PM03, PM04
uid___A002_X7d44e7_X14bc	17, 23 (97.5, 111.5)	2014-03-23 07:10	PM03, PM04
uid___A002_X7d6d46_X3c4	17, 23 (86.0, 100.0)	2014-03-24 06:34	PM03, PM04
uid___A002_X7d6d46_Xa98	17, 23 (97.5, 111.5)	2014-03-24 08:17	PM03, PM04
uid___A002_X7d76cc_Xb84	17, 23 (97.5, 111.5)	2014-03-25 03:39	PM03, PM04
Mars Band 6 data			
uid___A002_X79b541_Xf53	17, 21 (224.0, 240.0)	2014-01-28 06:09	PM01, PM03
uid___A002_X79b541_X115b	17, 21 (224.0, 240.0)	2014-01-28 06:40	PM01, PM03
uid___A002_X7a4b4d_Xe3b	17, 21 (224.0, 240.0)	2014-02-04 09:19	PM01, DV10
uid___A002_X7abc08_X1e6	17, 21 (224.0, 240.0)	2014-02-17 08:53	DA64, DV10
uid___A002_X7abc08_X518	17, 21 (224.0, 240.0)	2014-02-17 09:41	DA64, DV10
uid___A002_X7abc08_X835	17, 21 (224.0, 240.0)	2014-02-17 10:29	DA64, DV10
[b,c] uid___A002_X7daaaf_X1b28	17, 23 (228.0, 244.0)	2014-03-28 06:44	DA64, PM01, PM03, PM04
[b,c] uid___A002_X7daaaf_X2240	17, 23 (228.0, 244.0)	2014-03-28 08:03	DA64, PM01, PM03, PM04
[b,c] uid___A002_X7daaaf_X258b	17, 23 (247.0, 263.0)	2014-03-28 08:37	DA64, PM01, PM03, PM04
[b,c] uid___A002_X7e1b26_X1646	25, 35 (228.0, 244.0)	2014-04-01 05:37	DA64, PM01, PM03, PM04
[b,c] uid___A002_X7e1b26_X198e	39, 43 (247.0, 263.0)	2014-04-01 06:10	DA64, PM01, PM03, PM04

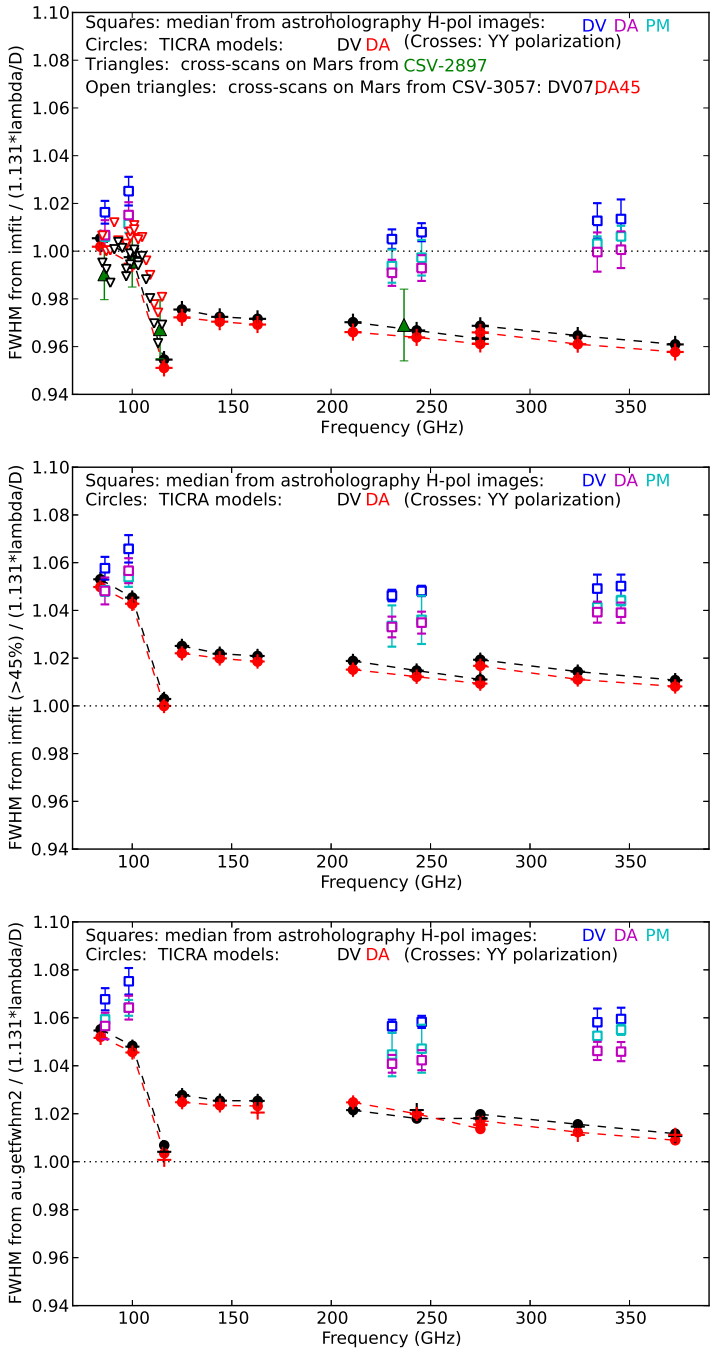

Fig. 10.— The FWHM of beam power patterns measured three different ways normalized by $1.131\lambda/D$. Top panel: plain CASA `imfit`, the triangles are from Gaussian fits to pol 0 cross-scans on Mars with the disk of Mars deconvolved from the result (from CSV-2897 and CSV-3057). Middle panel: `imfit` on pixels with intensity $> 0.45*$peak. Bottom panel: `au.getfwhm2`. The astroholography points and error bars are the median and standard deviation of all measurements within each antenna type, with the obviously bad datasets excluded. These plots were created with these three scripts: ticraHoloScale[Imfit/IncludePix].py.

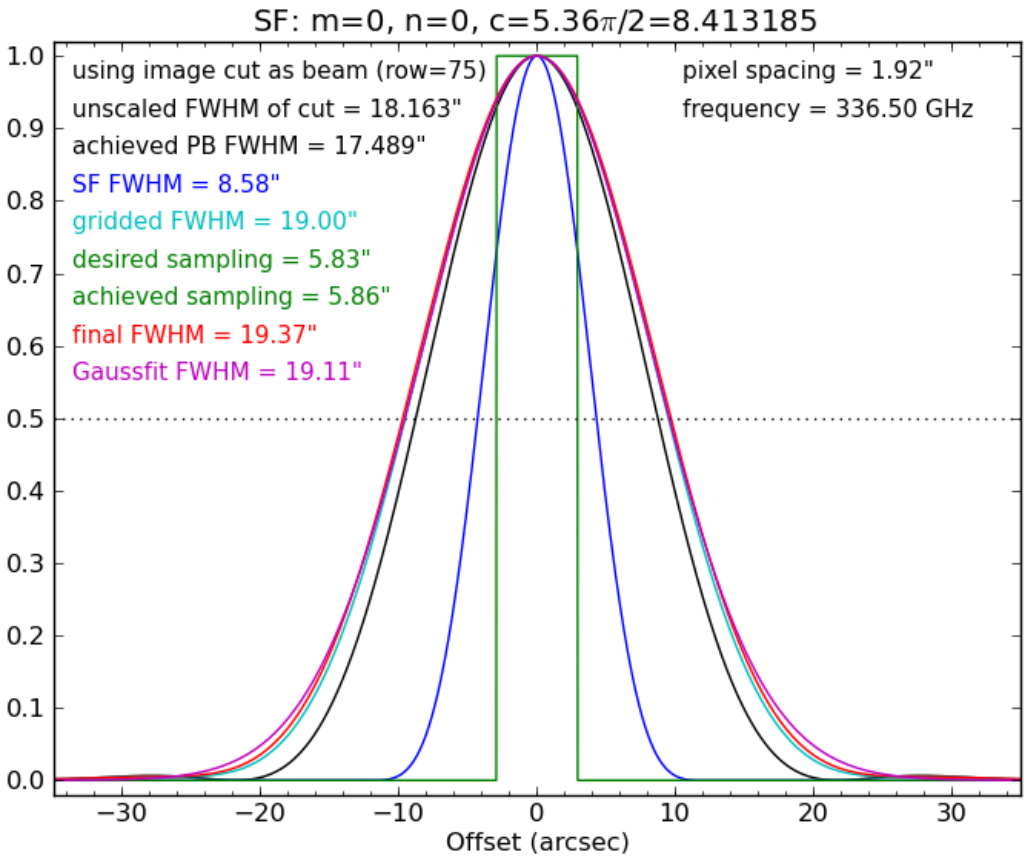

Fig. 11.— This plot summarizes the calculations of `au.sfBeam` using a DA TICRA model for the telescope primary beam in Band 7 (black line). The blue line shows the effective SF convolution function as defined by the `convsupport` parameter of 6, which corresponds to a FWZI of 12 pixels. Since the pixel spacing is 1.92″, the function goes to zero at ±11.52″. The convolution of the Gaussian and the SF is shown in cyan and has a FWHM=19.12″. The boxcar function shown in green represents the sampling interval on the sky of 5.77″ (1/3 of a beam), and the convolution of this with the cyan curve yields the red curve whose FWHM=19.52″. A Gaussian fit to this curve is shown in magenta which yields a slightly smaller FWHM=19.51″, and represents what the CASA task `imfit` would deliver. The angular size of the model has been automatically scaled to the requested frequency of 336.495 GHz by the frequency ratio. This plot was created with the command:

```
au.sfBeam(336.495, pixelsize=au.primaryBeamArcsec(frequency=336.495)/9.,
          xSamplesPerBeam=3.0, convsupport=6, makeplot=T,
          plotfile='sfBeam336GHzTicra.png',
          img='ALMA_0_DA__0_0_360_0_45_90_299.5_324_348.5_GHz_ticra2007_EFP.im')
```

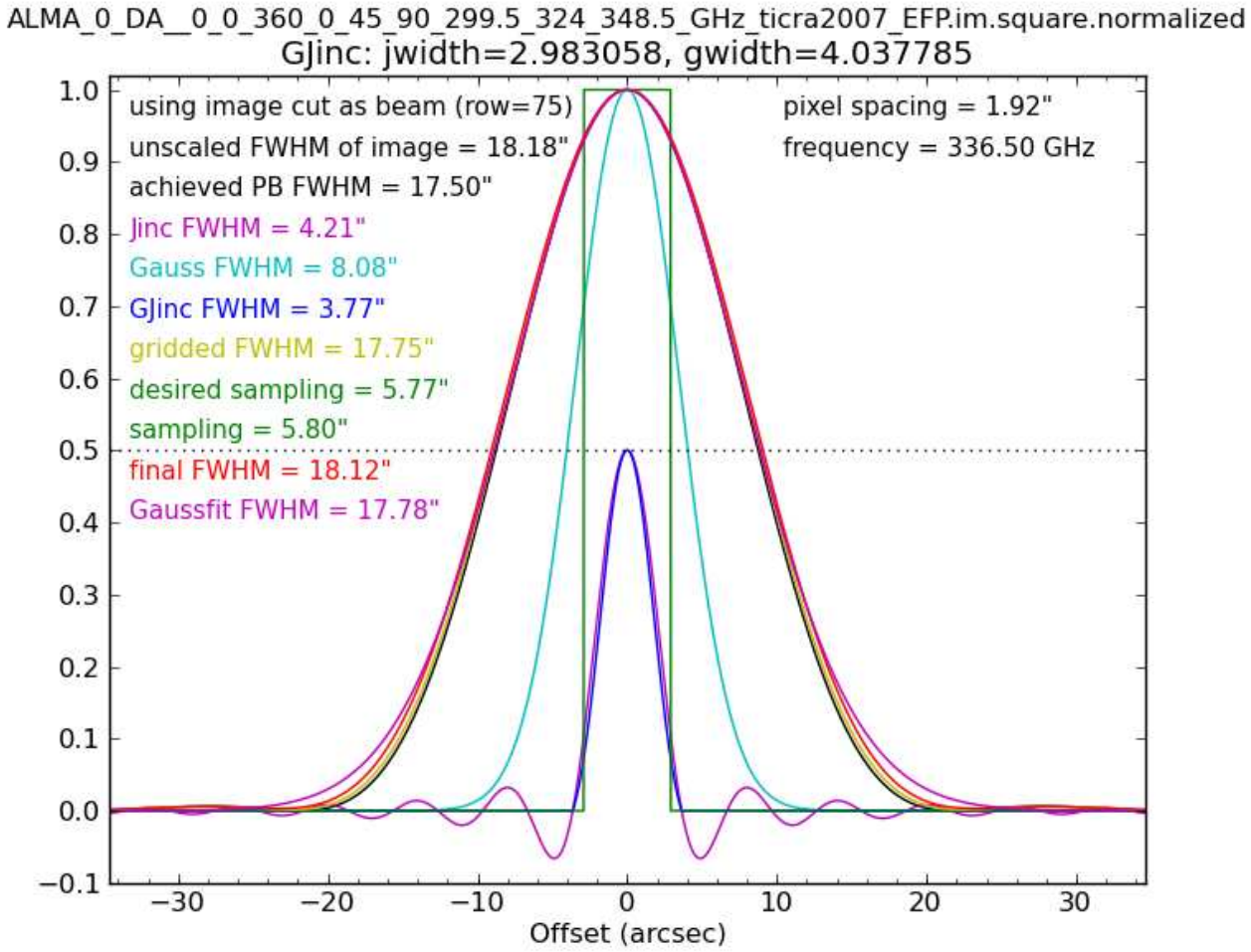

Fig. 12.— This plot summarizes the calculations of `au.gjincBeam`, which is analogous to `au.sfBeam`, but using the GJinc gridding function. The black line is the primary beam model, in this case the DA TICRA model. The magenta line peaking at y=0.5 is the Jinc function with a FWHM=4.21″. The cyan line shows the Gaussian profile which is multiplied by the Jinc function to obtain the GJinc function in blue with a narrower FWHM=3.77″ and truncated at the first null. The convolution of the primary beam with the GJinc is shown in yellow and has a FWHM=17.43″. The boxcar function shown in green represents the sampling interval on the sky of 5.77″ (1/3 of a beam), and the convolution of this with the yellow curve yields the red curve whose FWHM=18.07″. A Gaussian fit to this curve is shown in magenta which yields the same FWHM and represents what the CASA imfit function would deliver. This plot was created with the command:

```
au.gjincBeam(336.495, pixelsize=au.primaryBeamArcsec(frequency=336.495)/9.,
             xSamplesPerBeam=3.0,makeplot=T,plotfile='gjincBeam336GHz.png',
             img='ticraDA')
```

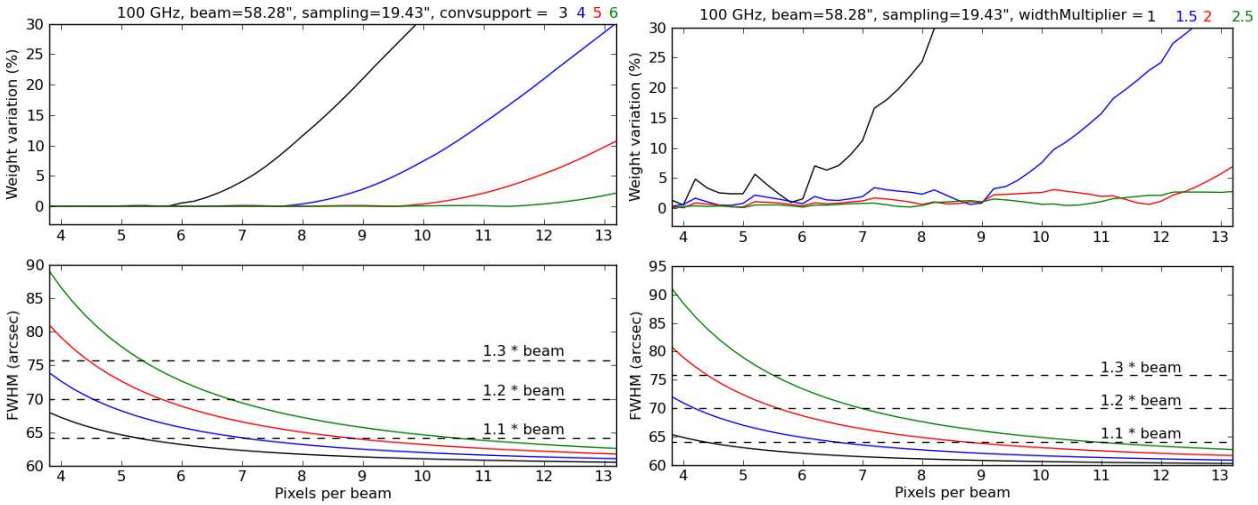

Fig. 13.— One-dimensional simulations at 100 GHz of the effect of gridding parameters on image weight and FWHM beam size assuming that the minimum sampling per beam is 3 for SF (**Left**) and GJINC (**Right**). **Upper panels:** The percentage variation in the weighted amount of data contributing to each pixel vs. the number of pixels per beam. The different colors correspond to four different choices of `convsupport` (for SF), or `gwm` (for GJINC). **Lower panels:** The FWHM of the predicted post-gridding beam. By combining the two plots, one can see that there is a limited range of useful values of pixels per beam for a given gridding function and parameters, as summarized in Table 2. This plot was created with the commands:
`au.sfBeamWeightVariation(100,samplesPerBeam=3,plotfile='sf_100GHz_samp3.png')`
`au.gjincBeamWeightVariation(100,samplesPerBeam=3,plotfile='sf_100GHz_samp3.png').`

5.2. Imaging and analysis script: grid_tests.py

Once the data were calibrated, in order to perform the imaging and analysis in a uniform manner, we wrote a script called `grid_tests.py`. Its functionality is described below.

5.2.1. Imaging

The script first creates a grid of 76 images for a specified dataset, spectral window (spw), and field using the SF grid function or the GJINC grid function. In both cases, we let the `cell` parameter range from 4.0 to 13.0 by 0.5 pixels per beam, where the theoretical beam is determined by `au.primaryBeamArcsec` using a taper that produces a FWHM of $1.131\lambda/D$, and the mean frequency of the spw. For the SF case, we let `convsupport` take values of 3, 4, 5 and 6. For GJINC, we apply the same multiplier to `gwidth` and `jwidth` and let it (gwm) take values of 1.0, 1.5, 2.0 and 2.5. Plots of the images are then produced using the `imview` task. In Figures 14 and 15 we show five SF images that demonstrate how only a certain

Table 3—Continued

Execution block	Spectral window (center freq. GHz)	Start Date/Time	Antennas
	Uranus Band 7 data		
[a] `uid___A002_X728403_X2c`	25, 29 (303.8, 292.0)	2013-11-12 03:07	DA62, DA64, PM01, PM04
[a] `uid___A002_X728403_X7e0`	25, 29 (303.8, 292.0)	2013-11-12 05:29	DA62, DA64, PM01, PM04
[d,g] `uid___A002_X8113a9_X370`	17,19,21,23 (337.4, 349.5)	2014-05-07 11:13	DA64, PM04
[e] `uid___A002_X81cc73_X656`	17,19,21,23 (337.4, 349.5)	2014-05-15 10:16	PM04
[e] `uid___A002_X81ddfc_X659`	17,19,21,23 (337.4, 349.5)	2014-05-16 10:43	PM04
[e,g] `uid___A002_X81ddfc_X9a3`	17,19,21,23 (337.4, 349.5)	2014-05-16 11:17	PM04
[e,f] `uid___A002_X82b2f1_X50b.ms`	19,21,23 (296.0, 308.0)	2014-05-28 10:23	DA64, PM03, PM04
[e,f] `uid___A002_X82b2f1_X73f.ms`	19,21,23 (296.0, 308.0)	2014-05-28 10:56	DA64, PM03, PM04
[e,f,g] `uid___A002_X82b2f1_X10ca.ms`	19,21,23 (296.0, 308.0)	2014-05-28 12:50	DA64, PM03, PM04

[a]These datasets were taken in ALMA software 9.1.3. Unmarked datasets were taken in 9.1R5.

[b]These datasets were taken in ALMA software 10.4. Unmarked datasets were taken in 9.1R5.

[c]These datasets are not shown in the Jy/K plot in §6 because Mars was too bright.

[d]These datasets were taken in ALMA software 10.6.0. Unmarked datasets were taken in 9.1R5.

[e]These datasets were taken in ALMA software 201404-CYCLE2-ON-B.

[f]Spw 17 was excluded due to PRTSPR-5361.

[g]Data acquired after sunrise.

range of cell sizes make sense for `convsupport` values of 3 and 6, respectively. Similarly, in Figures 16 and 17 we show five GJINC images that demonstrate how only a certain range of cell sizes make sense for gwm values of 1.0 and 2.5, respectively. The appearance of stripes or cross-hatching in the "weight" image is an indicator that the cell size is not appropriate.

5.2.2. Description of Analysis Script

After creating the images, the `grid_tests.py` script then calls `au.getTPSampling` on the measurement set in order to discern the sampling interval on the sky, because this important quantity is not otherwise available. These values are passed to the tasks `au.sfBeam` and `au.gjincBeam` which compute the predicted width of the beam for these gridding functions. These tasks are executed with the `img` option set to pick the nearest TICRA model image for the appropriate receiver band, and `stokes='both'`. Cuts through the TICRA images are automatically scaled in angular extent by the frequency ratio of the model frequency to the observed frequency of the chosen spw. By default, these functions each compute four FWHM quantities: (i) the FWHM of the predicted beam profile along the scan direction, (ii) the FWHM of the predicted beam profile along the perpendicular direction, (iii) the FWHM of a Gaussian fit to predicted beam profile along the scan direction, and (iv) the FWHM of a Gaussian fit to predicted beam profile along the perpendicular direction. The first value returned by the function is (1) the minimum of the first two FWHM quantities, i.e. the minor axis, which is typically the value from along the scan direction. The second value returned is (2) the maximum of the first two quantities, i.e. the major axis, and is typically the value from along the perpendicular direction. The third value returned is (3) the geometric mean of the first two return values (fwhmsfBeam). The fourth value returned is (4) the geometric mean of the third and fourth FWHM quantities (sfBeam), i.e. the mean FWHM of the Gaussian fit. The value of sfBeam is then written to the image header as the major and minor axes of the beam using the CASA toolkit function `ia.setrestoringbeam`. If the object is a planet, then the script uses `au.planet` to determine the planet angular diameter during the observation, and passes it along with sfBeam and fwhmsfBeam in two separate calls to `au.computeExpectedFWHM` to compute the expected FWHMs of the predicted beam.

The measured width of the beam was found in two ways: by fitting a Gaussian with the CASA task `imfit`, and with `au.getfwhm2`. First, the geometric mean of the major axis and minor axis in the dictionary returned by `imfit` (which is the fitted beam, not the deconvolved size) is computed and defined as Fitted_Beam. The result from `au.getfwhm2` is termed the FWHM_beam. We found that the Fitted_Beam depends on the portion of the data that is fit via the includepix parameter. We explored ranges from of 0-100% up to 90-100% of the peak and compare the resulting Fitted_Beam to FWHM_beam in Figure 18. When all of the data are used in the fit, the Fitted_Beam is too narrow by 2-4%, depending on the frequency band. Conversely, when too little of the data are used, the Fitted_Beam is

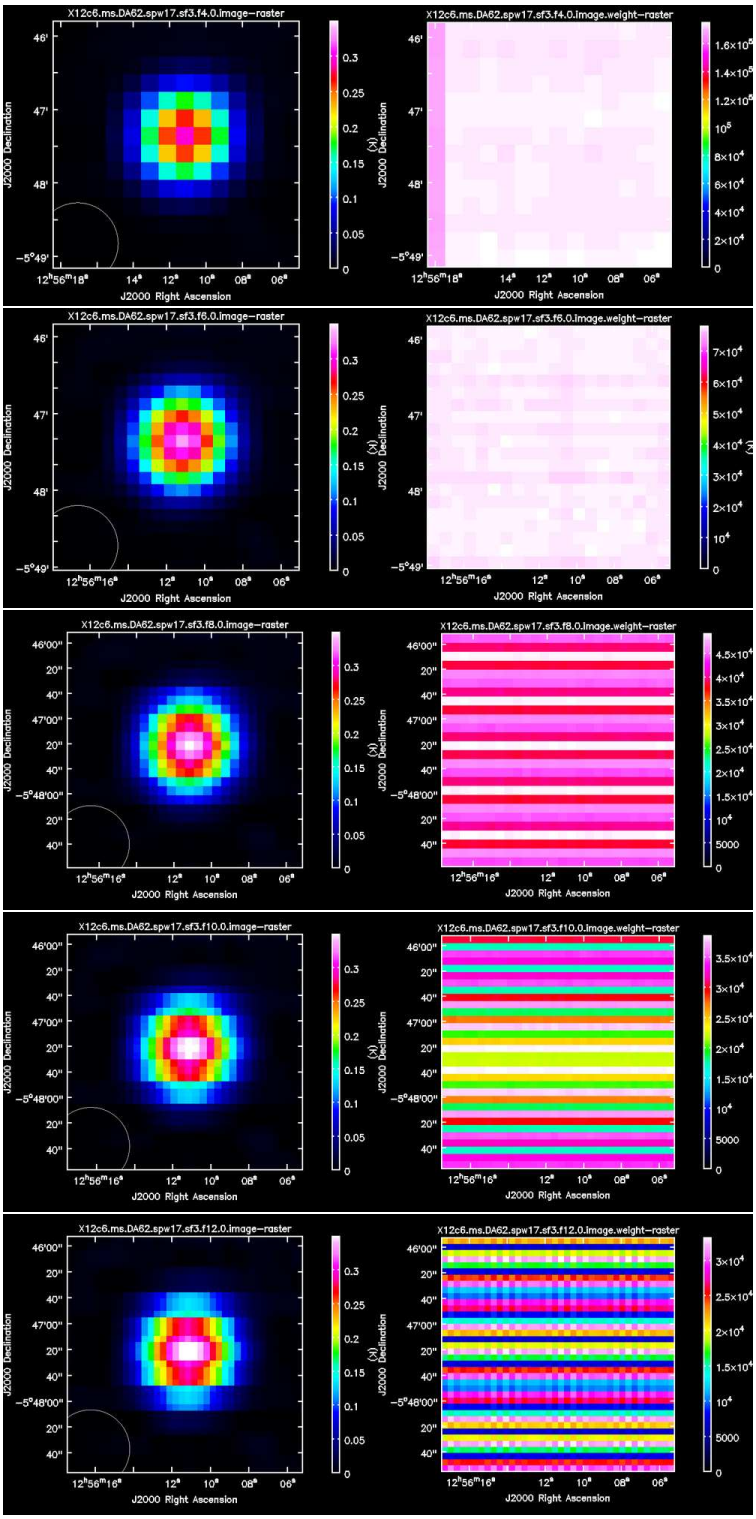

SF convsupport=3, pixels per beam=4.0

SF convsupport=3, pixels per beam=6.0

SF convsupport=3, pixels per beam=8.0

SF convsupport=3, pixels per beam=10.0

SF convsupport=3, pixels per beam=12.0

Fig. 14.— SF gridding with convsupport=3 (default) and pixels per beam = 4, 6, 8, 10, and 12. LEFT: 3c279 Band 3 image. RIGHT: Associated "weight" image.

too wide. The range of 45%-100% produces widths that are within 1% of the FWHM_beam.

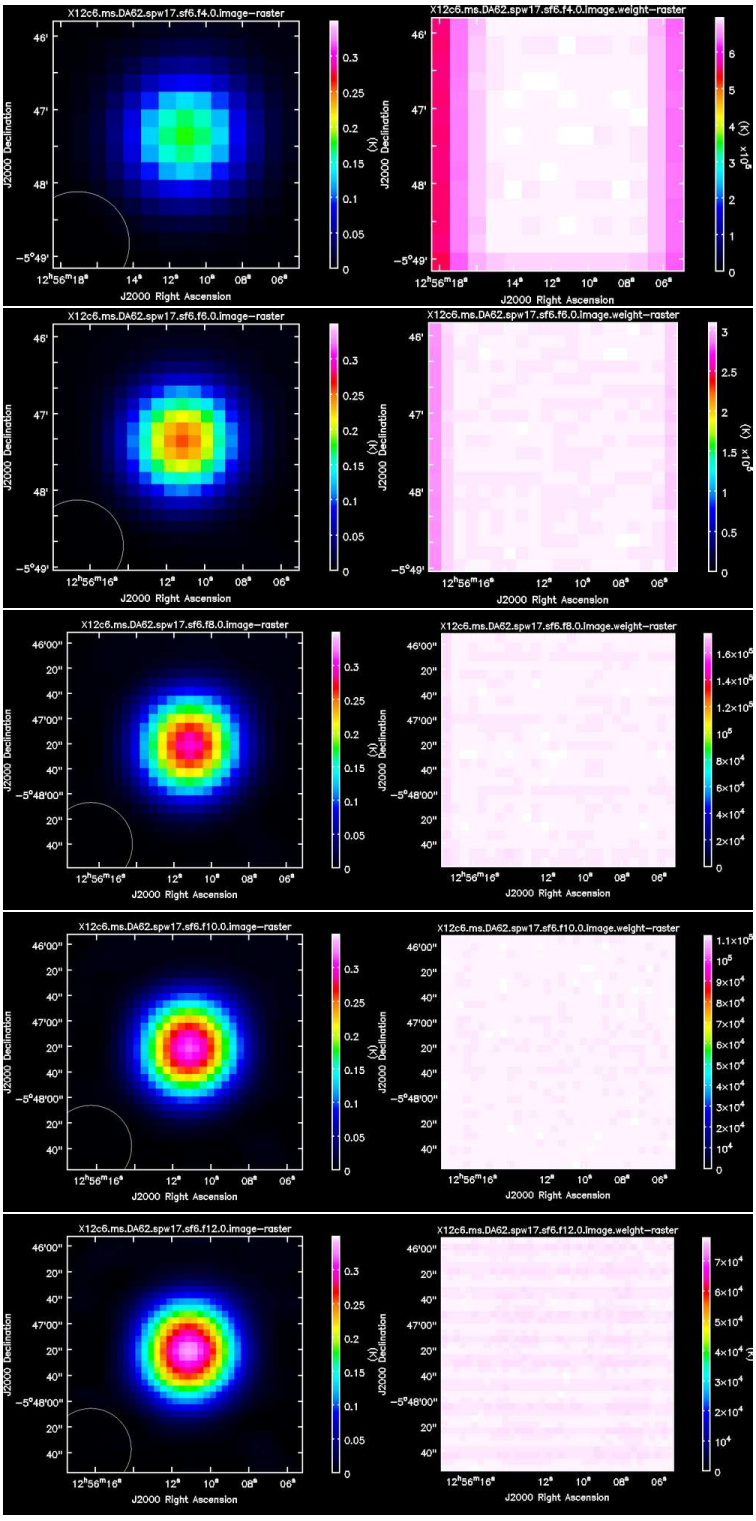

SF convsupport=6, pixels per beam=4.0

SF convsupport=6, pixels per beam=6.0

SF convsupport=6, pixels per beam=8.0

SF convsupport=6, pixels per beam=10.0

SF convsupport=6, pixels per beam=12.0

Fig. 15.— SF gridding with convsupport=6 and pixels per beam = 4, 6, 8, 10, and 12. LEFT: 3c279 Band 3 image. RIGHT: Associated "weight" image.

This range corresponds to using the pixels that are within 3.5 dB of the peak.

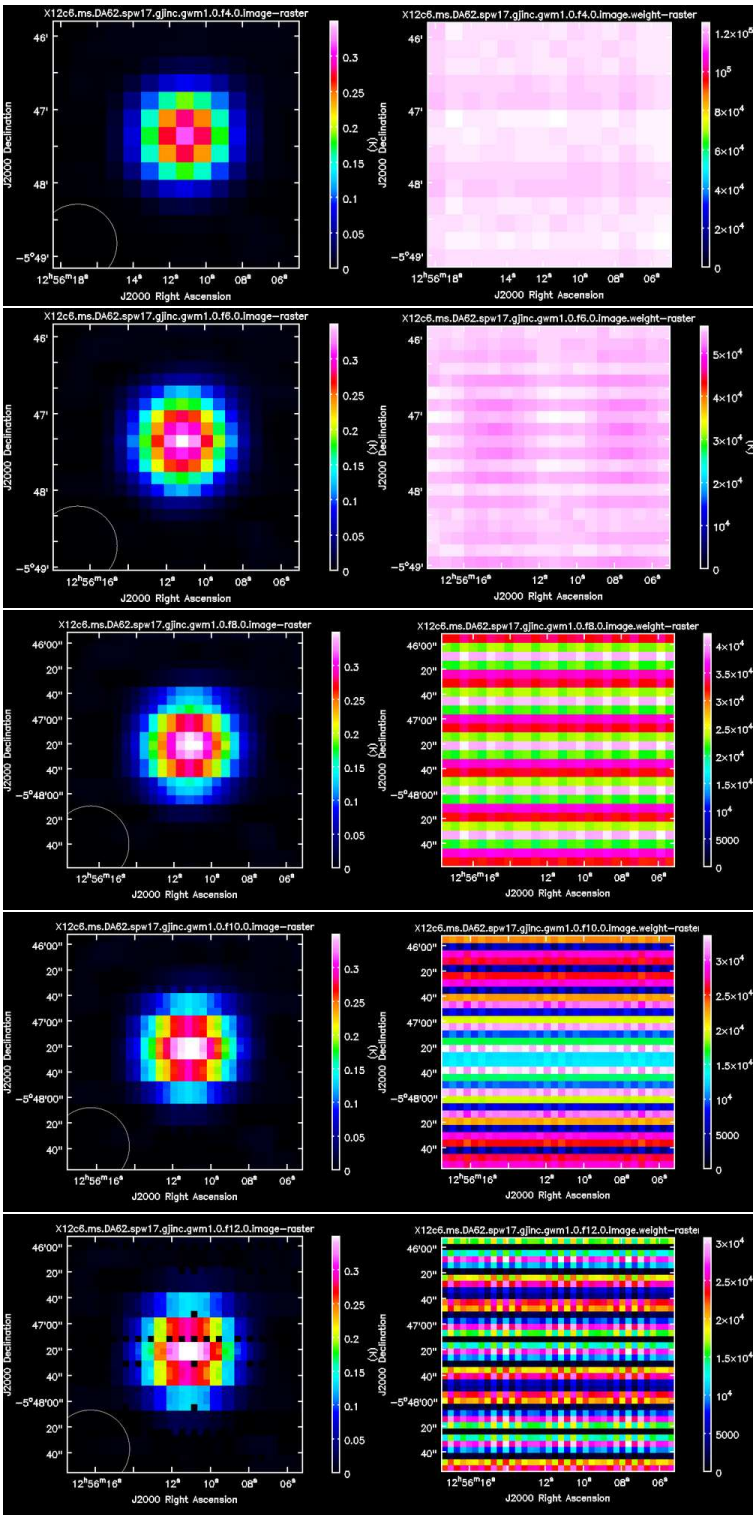

GJINC gwm=1.0,
pixels per beam=4.0

GJINC gwm=1.0,
pixels per beam=6.0

GJINC gwm=1.0,
pixels per beam=8.0

GJINC gwm=1.0,
pixels per beam=10.0

GJINC gwm=1.0,
pixels per beam=12.0

Fig. 16.— GJINC gridding with gwm=1 (default) and pixels per beam = 4, 6, 8, 10, and 12. LEFT: 3c279 Band 3 image. RIGHT: Associated "weight" image.

If the object is a planet, then the script runs `au.deconvolveDiskFromBeam` to determine

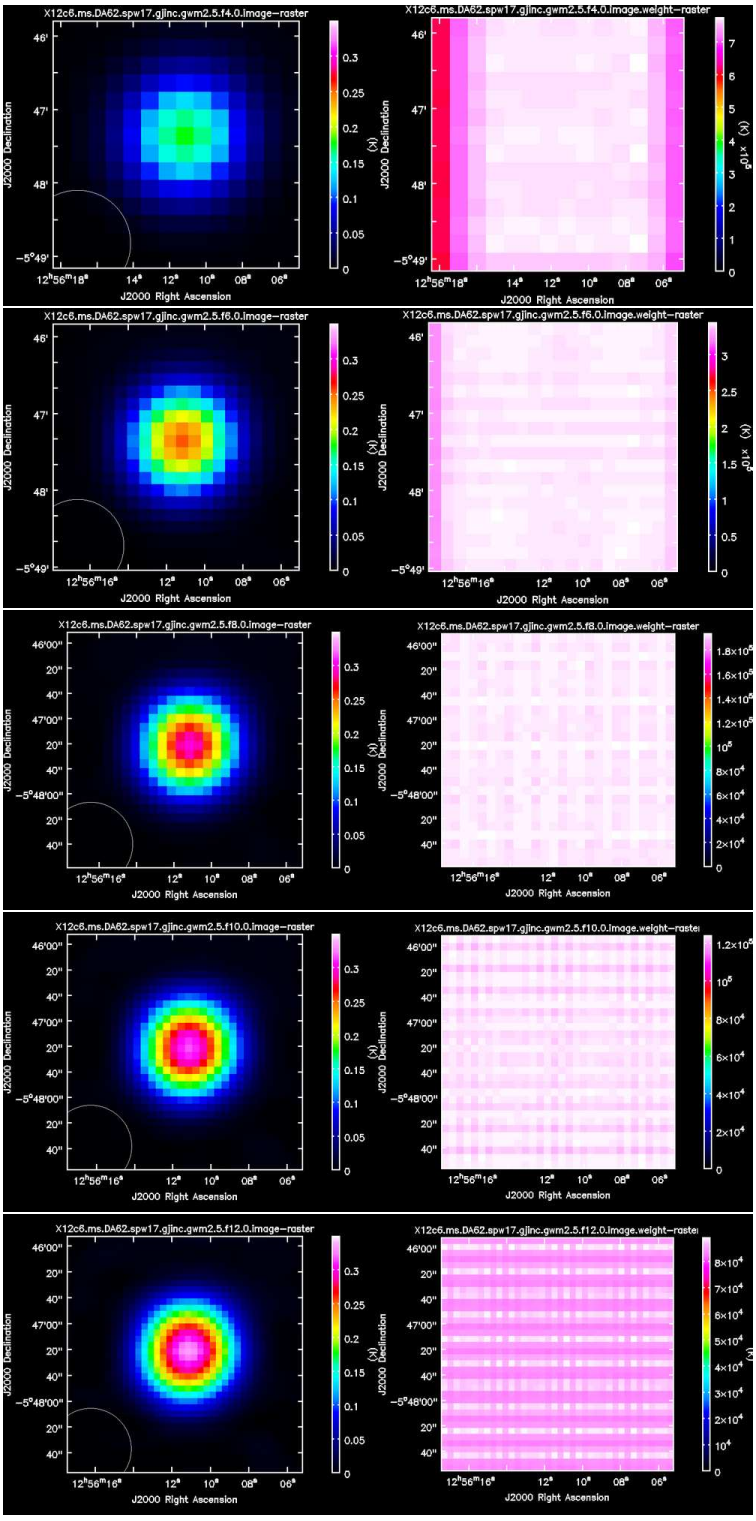

GJINC gwm=2.5, pixels per beam=4.0

GJINC gwm=2.5, pixels per beam=6.0

GJINC gwm=2.5, pixels per beam=8.0

GJINC gwm=2.5, pixels per beam=10.0

GJINC gwm=2.5, pixels per beam=12.0

Fig. 17.— GJINC gridding with gwm=2.5 and pixels per beam = 4, 6, 8, 10, and 12. LEFT: 3c279 Band 3 image. RIGHT: Associated "weight" image.

the underlying beam (called fittedcleanbeam). This beam is then used along with the fitted

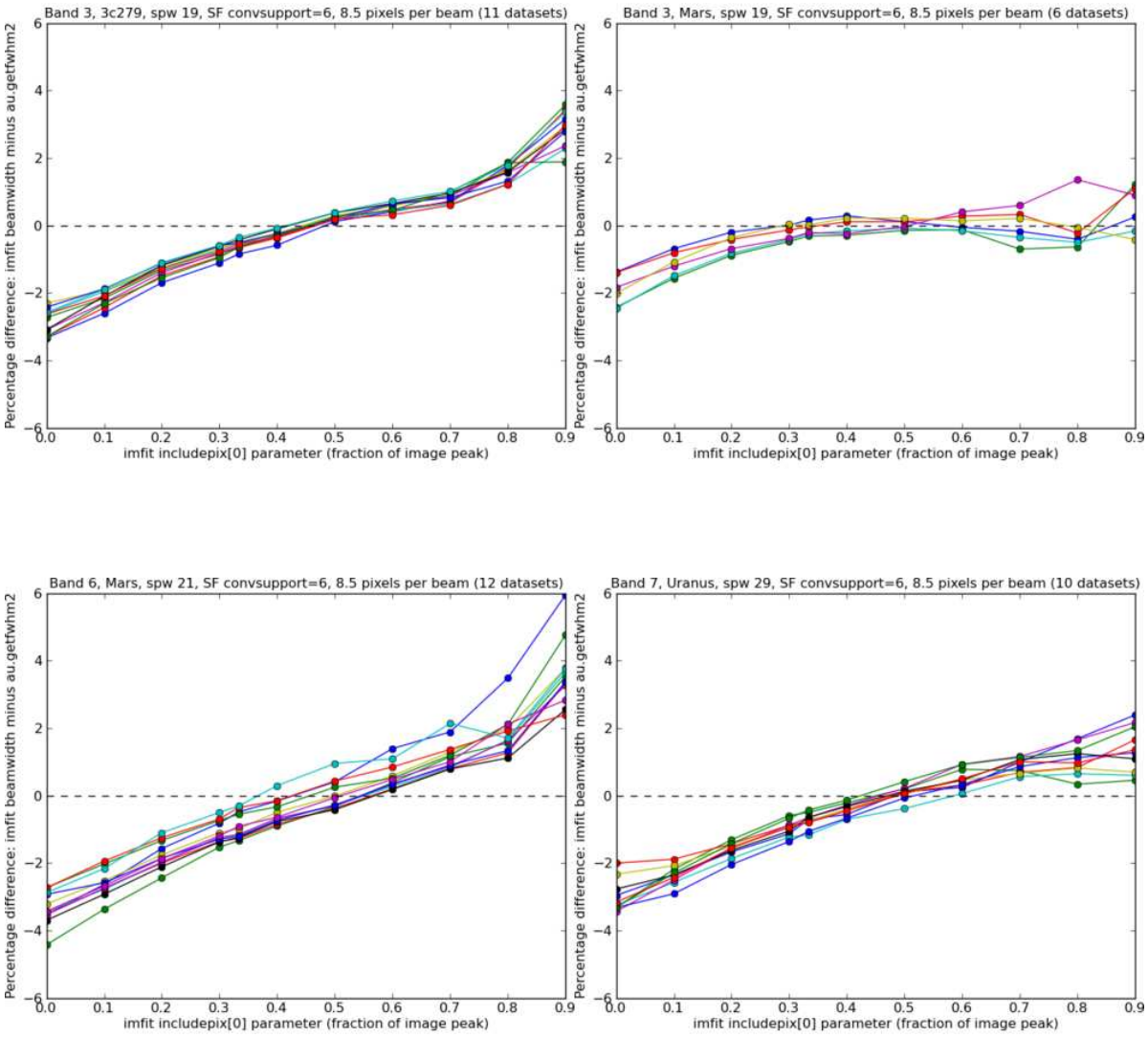

Fig. 18.— This plot shows the percentage difference between the beam width returned by `imfit` minus the width returned by `au.getfwhm2` for the case of convsupport=6 and 8.5 pixels per beam. The upper left plot is 3C279 at Band 3, upper right is Mars at Band 3, lower left is Mars at Band 6, and lower right is Uranus at Band 7. The different colored points correspond to different datasets taken at different times and/or with different antennas.

flux from `imfit` to compute the fitted flux in units of Kelvin*beam (called fitted_flux_KB). The script then uses sfBeam along with the fitted flux from `imfit` to compute the predicted fitted flux in units of Kelvin*beam (called predicted_fitted_flux). The script also analyzes the images using the CASA task `imstat` to find the peak and the rms. The rms is found within an annulus centered on the image center with an inner radius of 1.5 beamwidths and

an outer radius of 3.5 beamwidths. The signal to noise ratio (snr) is then computed from the ratio of peak to rms.

5.2.3. Results of Analysis Script

The quantitative results for the 3c279 Band 3 data from DA62 using the SF compared to GJINC `gridfunction` are shown in Figure 19. The results for the Uranus Band 7 data from PM01 is shown in Figure 20. In each of these figures, there are two nine-panel plots, each of which contain the following information. The values of peak, rms, and snr are shown in the first 3 panels of the figures (top row). The value of sfBeam is shown in the 4th panel and the ratio of sfBeam to Fitted_Beam is shown in the 5th panel. The ratio of sfBeam to FWHM_Beam is shown in the 6th panel. The value of predicted_fitted_flux is shown in the 7th panel, fitted_flux_KB is shown in the 8th panel, and their ratio is shown in the 9th panel. The general trends are as follows: (i) the image peak intensity increases with pixels per beam and asymptotes to a common value, (ii) the rms increases gently with pixels per beam, (iii) the snr shows a broad maximum with respect to pixels per beam which increases as the support parameter is increased, (iv) the predicted beam drops as pixels per beam increases, (v) the ratio of predicted to fitted beam is close to unity but with a gentle slope vs. pixels per beam, (vi) the ratio of predicted to FWHM_beam is close to unity but with more scatter at larger values of pixels per beam, (vii) the predicted flux increases with pixels per beam, (viii) the fitted flux increases with pixels per beam and asymptotes to a common value, (ix) the ratio of fitted to predicted flux follows the square of the ratio of predicted to fitted beam.

In general, for both the SF and GJINC gridding fucntions, we see the expected trends in the peak temperature and beamwidth as a function of the number of pixels per beam. In Band 3, we find that predicted beam agrees with the fitted beam to about 3%, and subsequently, the predicted flux agrees with the fitted flux to about 6%. The same is true in Band 7 when the convsupport is set to 6. We also see that the SNR goes through a peak at or near the optimal value of pixels per beam as previously shown in Figure 13.

6. Jy/K Conversion Factor

This section is still in draft form. Calibrated SD images will have units of brightness temperature. When combining SD and interferometric images, the CASA task `feather` requires that the images have the same flux density normalization scale. Therefore, the SD image must be converted to Jy/beam using the telescope gain conversion factor (Jy/beam per K). Because the gains are not well measured for all antennas and they can vary with frequency within a band, and with observing conditions in the higher bands, the ObsMode working

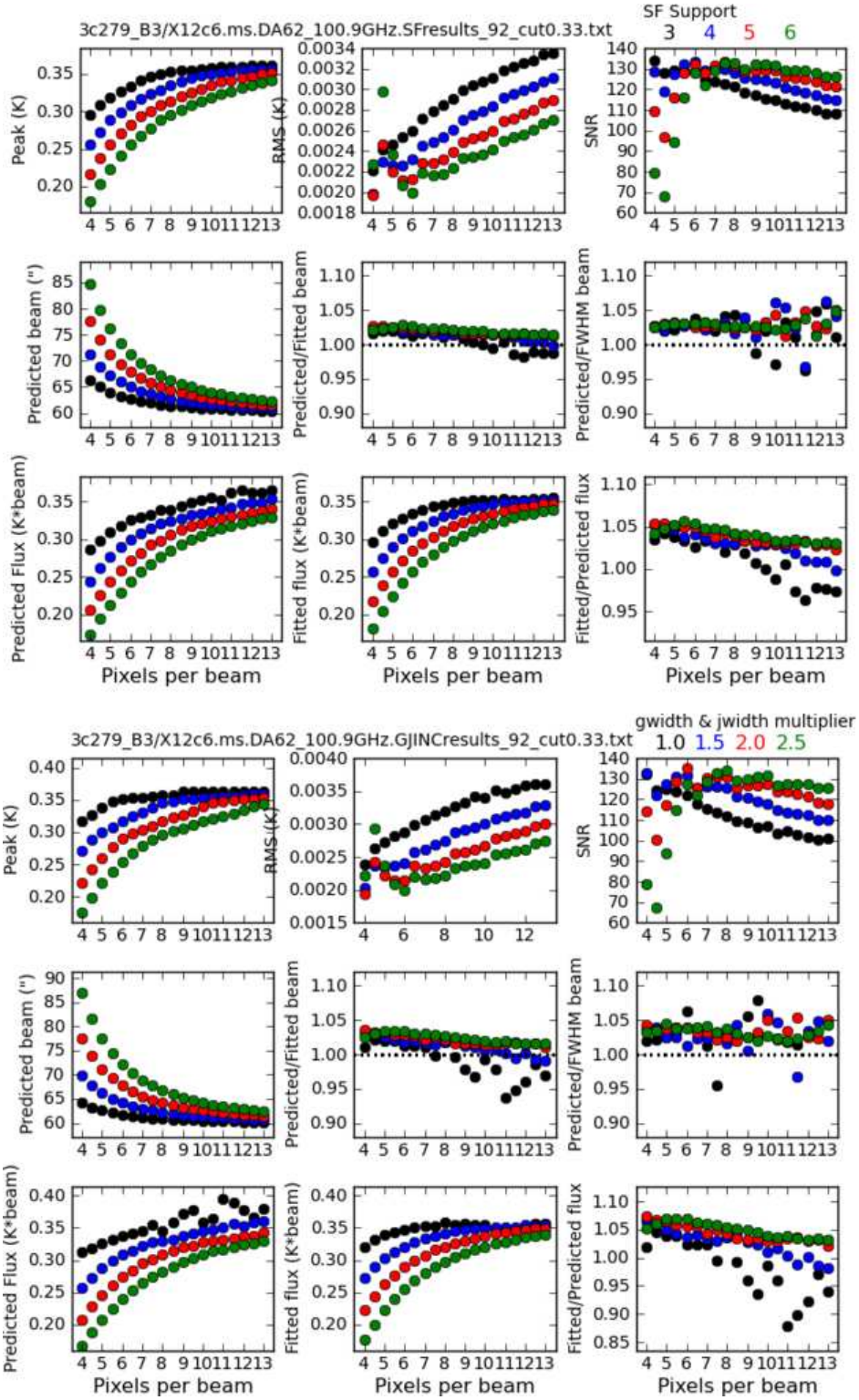

Fig. 19.— Summary of image analysis for SF (top) and GJINC (bottom) gridding functions for a 3c279 Band 3 dataset and DA62 (uid__A002_X725175_X12c6).

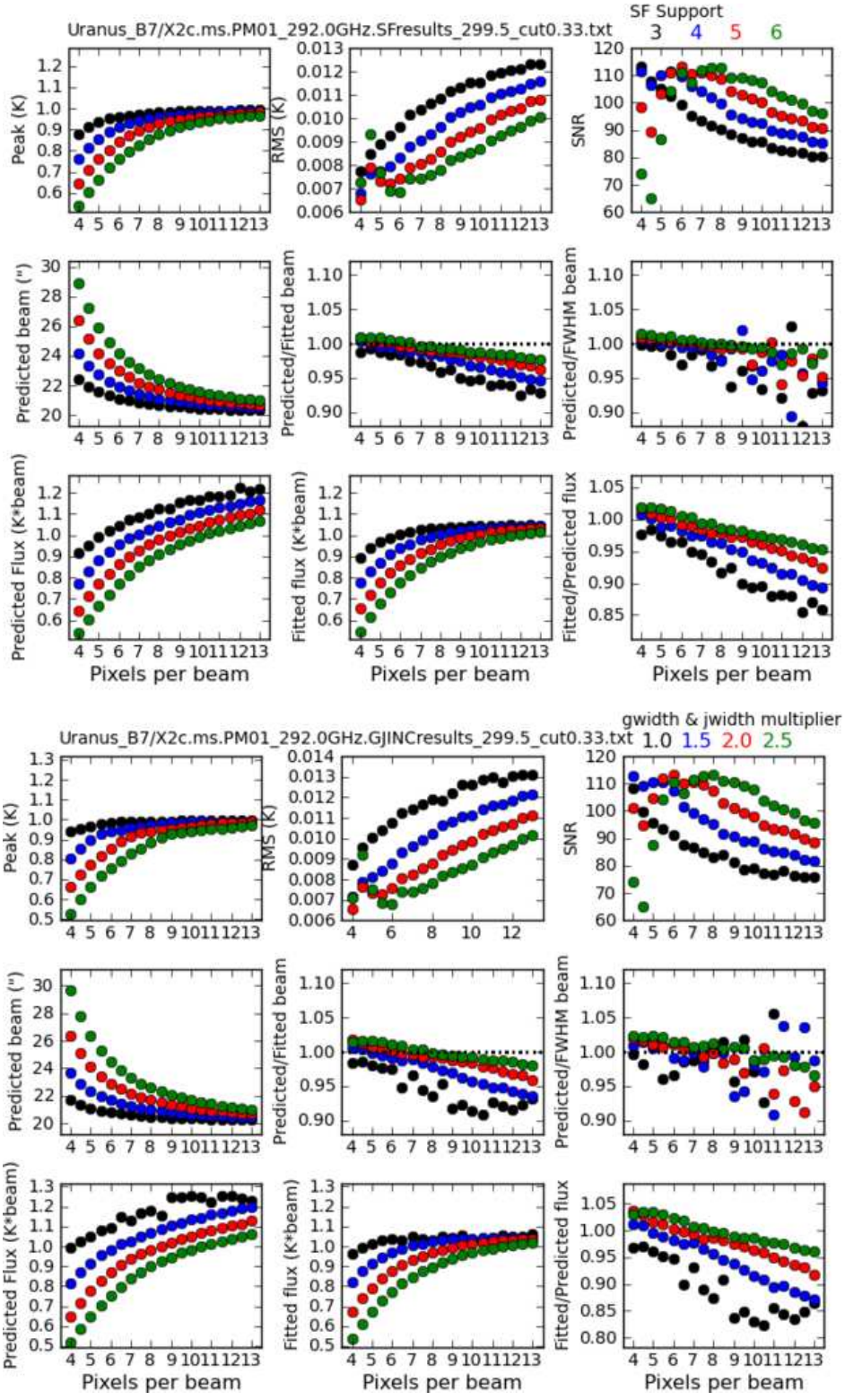

Fig. 20.— Summary of image analysis for SF (top) and GJINC (bottom) gridding functions for a Uranus Band 7 dataset and PM01 (uid__A002_X728403_X2c).

group decided that for Cycle 1 (and 2), we will obtain an image of the amplitude calibrator (SD-cal) for each total power project. This image will be acquired with an independent scheduling block from the science field, because an appropriate object may not be available at the same LST as the science target. We will use this image along with either the calibrator's model flux density in CASA (for Solar System objects) or its measured flux density from the ALMA calibrator database (for quasars) to determine the gain of each antenna for each SD observation. It is critical that the SD-cal data and science data be imaged with identical control parameters in `sdimaging`. Also, for non-point source calibrators, one cannot simply determine the conversion factor by taking the peak brightness temperature – one must measure the total emission in the image which requires accurate knowledge or prediction of the beam size as described in § 4.

The theoretical conversion factor (G) for the raw data depends on the antenna effective area (in cgs units), which in practice may vary from antenna to antenna:

$$\text{Gain (Jy/K)} \equiv G = \frac{2k}{A_{\rm eff}} \times 10^{23} \tag{1}$$

The equation for the antenna efficiency area contains the Ruze formula and can be found in the ALMA Technical Handbook section 9.2.1:

$$\eta = R_0 \exp(-16\pi^2\sigma^2/\lambda^2), \tag{2}$$

where σ is the rms surface accuracy of the antenna (with a specification of 25 μm for the 12m antennas) and $R_0 = 0.72$. Hence the effective area is:

$$A_{\rm eff} = \pi(D_{\rm dish}/2)^2\eta = \pi(D_{\rm dish}/2)^2 R_0 \exp(-16\pi^2\sigma^2/\lambda^2). \tag{3}$$

The equation for G thus reduces to:

$$G = 33.910 \exp(-0.0987/\lambda^2_{\rm mm}). \tag{4}$$

However, as we have seen in §3, the imaging process expands the effective beam size ($\theta_{\rm image}$) relative to the antenna beamsize ($\theta_{\rm antenna}$), which will expand the conversion factor accordingly by the change in beam area:

$$\begin{aligned} \text{Gain}_{\rm image}\text{(Jy/K)} \equiv G' &= G\left(\frac{\theta_{\rm image}}{\theta_{\rm antenna}}\right)^2 = G\left(\frac{\theta_{\rm image,arcsec}}{19.428\lambda_{\rm mm}}\right)^2 \\ &= 35.936\left(\frac{1}{\lambda_{\rm mm}}\right)^2\left(\frac{\theta_{\rm image,arcsec}}{20''}\right)^2 \exp\left(\frac{+0.0987}{\lambda^2_{\rm mm}}\right). \end{aligned} \tag{5}$$

Equation 5 is implemented in `au.janskyPerKelvin`, which takes as input the observing frequency and the image beamsize after gridding.

In Figure 21, we plot the observed value of the gain for each of the analyzed images, using the known flux density of the calibrator. For planets, the plotting script uses `au.planetFlux` which consults the CASA models (Butler 2012), and for quasars it uses `au.getALMAFluxForMS` which consults the online ALMA calibrator database to determine the most recent measurements in Bands 3 and 7, computes the spectral index, and interpolates to the desired frequency. A correction factor of 1/1.29 for the ACA non-linearity was applied to the derived Jy/K for each data point, as derived in a spreadsheet by T. Kamazaki (CSV-2880: csv-2880_thcf_20140331.xlsx). In other words, the ACA data in Kelvin must be multiplied by a correction factor of ~ 1.29 to be comparable to data from other single dish telescopes that do not suffer from the compression problem. It is important to note that this value is heavily dependent on the input power levels, and 1.29 is simply the value expected if the levels had been set optimally and they did not change during the raster map, including when passing through the target calibrator. It is recognized that the online system, even if operating perfectly, the input power levels will typically deviate by ± 0.5 dB from the optimal level simply due to the quantization of the attenuators and the optimization algorithm in the control software. To assess how well the online system is doing, we wrote an analysisUtils class called SQLD to query the TMCDB and the computing logs to read the SQLD voltages and the individual gain coefficients in order to convert them to milliwatts and then to dBm. In the May 2014 data, we find that the ACA datasets do seem to be within about 0.5 dB from the target of +2.4 dBm. However, we discovered that the baseline correlator datasets taken in mixed mode use an average target of +3 dBm which is sub-optimal for both FDM and TDM basebands (Comoretto 2008). A ticket was created to allow individual setting of baseband target levels (ICT-3041).

For comparison to the imaging results, in Figure 21 we also show the theoretical gain of the antenna beam prior to imaging (solid stars), and the theoretical gain with the chosen imaging parameter (open stars) using equation 5. The theoretical gains are computed two ways: in the top panel the value from `au.sfBeam` is used as $\theta_{\rm image,arcsec}$, so there is only one prediction per antenna type. In contrast, in the bottom panel, the value from `imfit` is used which has a unique value for each dataset. (Note that we fit to the data above 45% of the peak as described in § 5.2.2). The centroid of the predictions in general agree with the centroid of the observations, although there is significant scatter between datasets and antennas. In Figure 21, the nearest TICRA model to the observing frequency was used, with its size scaled by the frequency ratio of the model. In light of the results in § 3.3 (Figure 10), the Band 3 points were calculated using the 125 GHz TICRA model in au.sfBeam. The origin of the remaining scatter has not been investigated in detail, but it does not appear to be simply due to elevation or ambient temperature as many of the datasets showing scatter were taken consecutively. We note that the scatter was initially worse, with some datasets exhibiting systematic outliers. Subsequent investigations showed that the Tsys measurements were anomalous and were recomputed using offline casapy-telcal which resulted in more reasonable values, and brought the points into better agreement. There

has been no attempt to try to perform individual Ruze calculations based on individual antenna surface accuracy measurements. To our knowledge, the effective surface accuracy as measured at the AOS has not been tabulated on an antenna by antenna basis.

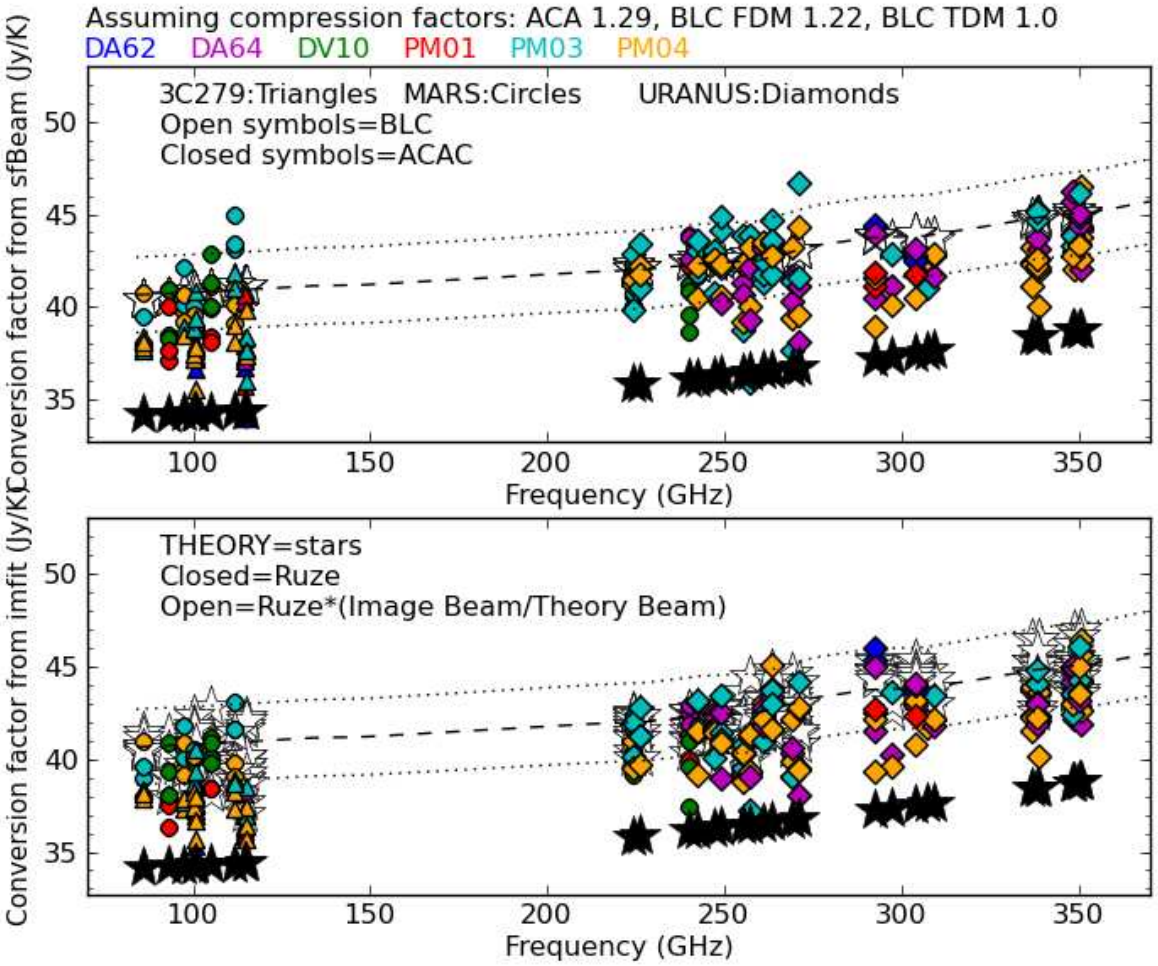

Fig. 21.— This figure shows the Jy/K conversion factor for the images generated from all of the ACA correlator data shown in Table 3 (except for those excluded by table note c). The **TOP** panel shows Jy/K derived from `sfBeam`, using the TICRA model from the nearest frequency. The **BOTTOM** panel shows Jy/K derived from the `imfit` beam. In both panels the black filled stars show the theoretical Jy/K using the native antenna beam, while the open stars show the "post-imaging" Jy/K (i.e corrected for the broadening of the beam during imaging). The dashed line is the expected value based on the Ruze formula and the expected beamsize after imaging. The dotted lines are ±5% around the dashed line. To avoid confusion, no results from the baseline correlator are shown.

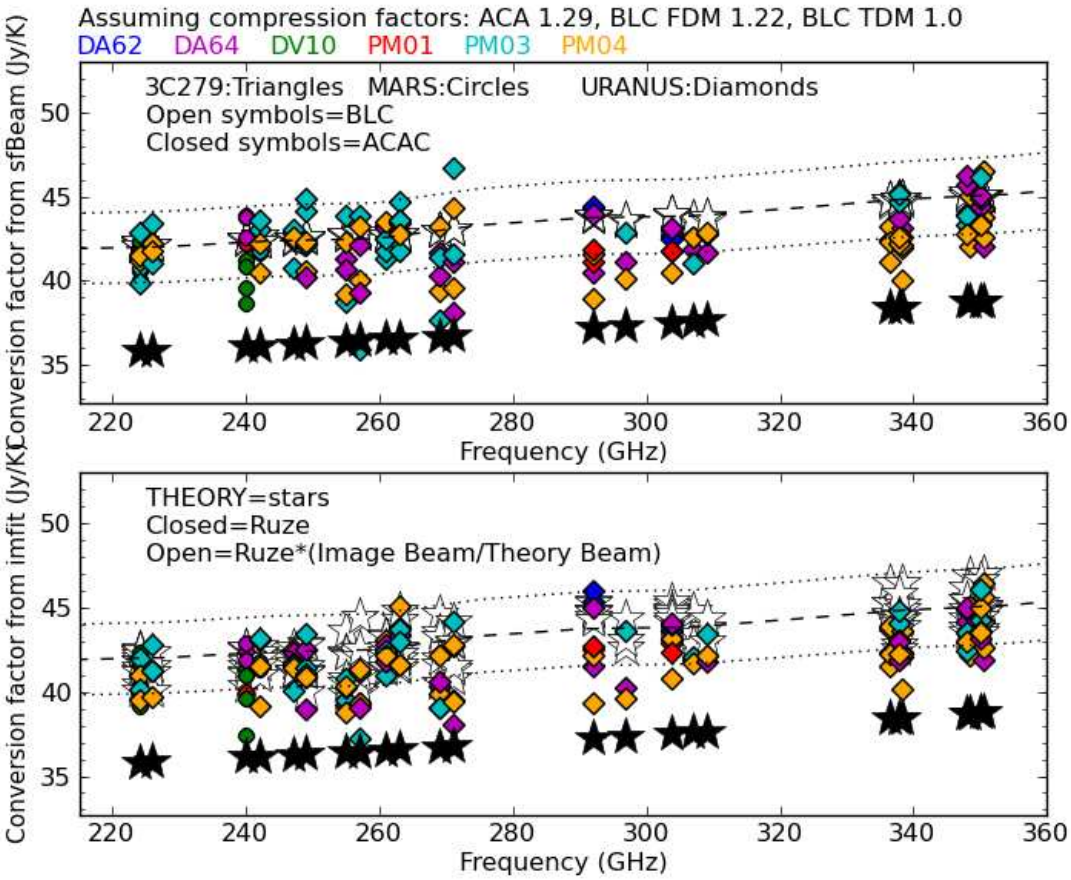

Fig. 22.— Same as Fig. 21, except zoomed in frequency to show Bands 6 and 7 in more detail. To avoid confusion, no results from the baseline correlator are shown.

7. Primary beam in CASA

CASA currently (v4.2.1) uses a truncated Airy pattern (truncated at the first null) for the ALMA beam for both cleaning tasks and simulation tasks (see JIRA ticket CAS-5806). As we have seen in this memo, this pattern is not a good representation of the ALMA beam. Its historical usage can be ascribed to the fact that the VLA antennas have non-hyperbolic (i.e "shaped") secondary mirrors which provide nearly uniform illumination of the primary mirror (see § 4.1.4 of Napier 1989), resulting in beam profiles close to Airy in shape. For ALMA antennas, CASA uses a primary mirror diameter of 10.7 m instead of 12 m (and 6.5 m instead of 7 m for the CM antennas) when applying the Airy formula. These reduced diameters were implemented in JIRA ticket CAS-3532 in order that the FWHM of the truncated Airy better agrees with the FWHM of the actual ALMA beam. An improvement to the ALMA beam used in CASA tasks will need to be made in the future, and will likely use the TICRA models. Initial tests have been run using the CASA

toolkit, in which the voltage pattern can be specified with `vp.setpbimage`. However, this feature is computationally intensive and `im.clean` takes much longer to run. Since it is likely that much of the improvement could be gained by using an axisymmetric profile, we have computed such a profile for the TICRA 100 GHz model image and sent the resulting ASCII file to the CASA developer for testing (see Figure 23). In the future as more information becomes available (for example from astroholography), it will be possible to use observed antenna patterns (or averages thereof, probably per antenna type).

8. Acknowledgements

We thank D. Petry for help with the TICRA images. We thank M. Sugimoto, E. Fomalont, and R. Lucas for providing information on the astroholography data. We thank B. Dent for pointing out the results from CSV-2897. Finally, we thank B. Mason for writing the initial version of `au.getfwhm`.

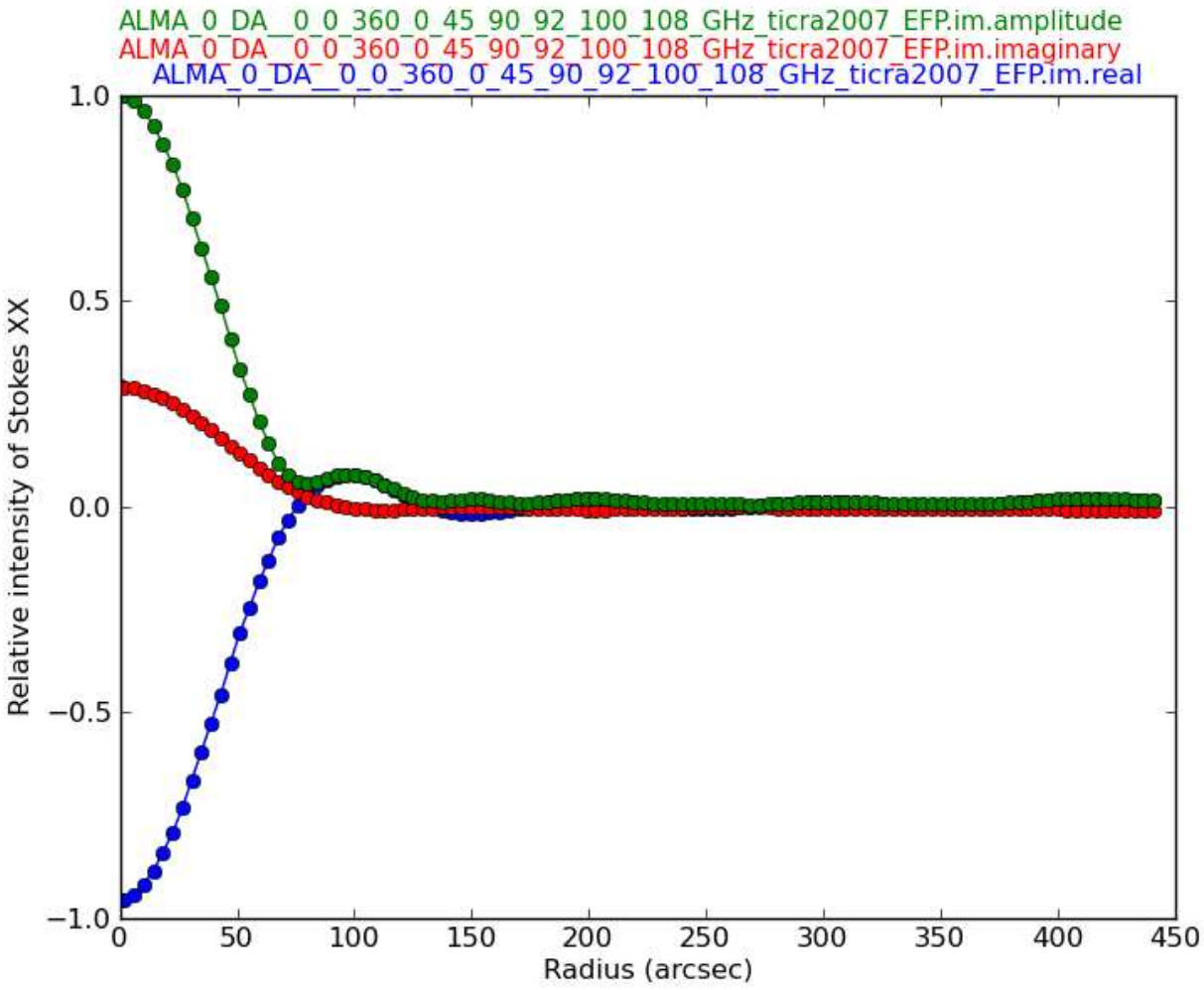

Fig. 23.— Axisymmetric complex voltage pattern as modeled by TICRA for the DA antennas X polarization at 100 GHz sent to the CASA developers as an ASCII table in February 2014 (CAS-3532). The command used to generate this profile and create the plot was:

```
au.extractAzimuthalAverageFromImage(
    'ALMA_0_DA__0_0_360_0_45_90_92_100_108_GHz_ticra2007_EFP.im.real',
    'ALMA_0_DA__0_0_360_0_45_90_92_100_108_GHz_ticra2007_EFP.im.imaginary',
    'ALMA_0_DA__0_0_360_0_45_90_92_100_108_GHz_ticra2007_EFP.im.amplitude',
    stokes='XX',outfile='band3_DA_XX.dat',
    maxradius=180,interpolateToZero=True,
    peakimage='ALMA_0_DA__0_0_360_0_45_90_92_100_108_GHz_ticra2007_EFP.im.amplitude',
    plotfile='band3_DA_XX.png')
```

9. References

- Albertsen, N. Chr., "Optimization of warm optics for Band 3 front end for ALMA", February 2009, FEND-40.01.03.00-012-A-REP

- Baars, J.W.M., "The Paraboloidal Reflector Antenna in Radio Astronomy and Communication", Berlin: Springer, 2007
- Butler, B. et al. 2006, "Calibration Specifications and Requirements", ALMA-90.03.00.00-001-A-SPE version D, 2006-05-18
- Butler, B., Flux Density Models for Solar System Bodies in CASA", ALMA Memo 594, November 2012, https://science.nrao.edu/facilities/alma/aboutALMA/Technology/ALMA_Memo_Series/alma594/memo594.pdf
- Carter, M. et al, "ALMA Front-End Optics Design Report", FEND-40.02.00.00-035-B-REP, 2007-03-30
- Comoretto, G. "Algorithms and formulas for hybrid correlator data correction", ALMA Memo 583, November 2008, http://www.arcetri.astro.it/science/Radio/alma/ALMA_Memo_583.pdf
- Cornwell, T.J., Holdaway, M.A. & Uson, J.M. 1993, A&A, 271, 697
- Mangum, J., Emerson, D., Greisen, E., 2007, A&A, 474, 679
- Morita, K.-I. et al., "ALMA System Technical Requirements", ALMA-80.04.00.00-005-C-SPE, 2012-12-10
- Napier, P.J., 1989, "Synthesis imaging in radio astronomy", p. 39
- Petry, D., "Antenna responses for ALMA in CASA", Seventh SKA Workshop on Calibration and Imaging (CALIM 2012), December 2012, available at http://calim2012.ska.ac.za/programme
- Pontoppidan, K, "Electromagnetic properties and optical analysis of the ALMA antennas and Front Ends", October 2007, available at www.nrao.edu/ demerson/alma-feic/2007-10-04_optical_analysis_final_report_chapter_5.pdf
- Rhodes, D.R., 1970, Journal of Research of the National Bureau of Standards – B. Mathematical Sciences, Vol 74B, No. 3
- Schroeder, D.J., "Astronomical Optics", San Diego: Academic Press, 1987
- Schwab, F., 1981, VLA Computer Memorandum 156, "Rational Approximations to Selected 0-order Spheroidal Functions".
- Sørensen, S., & Pontoppidan, K. 2010, Twenty-First International Symposium on Space Terahertz Technology, p. 121 (ADS: 2010stt..conf..121S)

Appendices

The analysisUtils (au) python functions described in this memo are available as a tarball from the CASAguide webpages:

http://casaguides.nrao.edu/index.php?title=Analysis_Utilities

The most up-to-date documentation for the following functions (among hundreds of others) is kept on the NRAO external wiki at https://safe.nrao.edu/wiki/bin/view/Main/CasaExtensions.

- au.complexToSquare
- au.computeExpectedFWHM
- au.deconvolveDiskFromBeam
- au.findFWHM
- au.getfwhm2
- au.getALMAFluxForMS
- au.getTPSampling
- au.gjincBeam
- au.janskyPerKelvin
- au.planet
- au.planetFlux
- au.primaryBeamArcsec
- au.antennaEfficiency
- au.sfBeam
- au.sfBeamWeightVariation
- au.pickTicraImage
- au.SQLD (class)
- au.griddedBeam (class)